1965

Nucleosynthesis of Heavy Elements by Neutron Capture

Philip A. Seeger
California Institute of Technology

William A. Fowler
California Institute of Technology

Donald D. Clayton
Clemson University, claydonald@gmail.com

NUCLEOSYNTHESIS OF HEAVY ELEMENTS BY NEUTRON CAPTURE*

PHILIP A. SEEGER† AND WILLIAM A. FOWLER
California Institute of Technology, Pasadena, California
AND
DONALD D. CLAYTON
Space Science Department, Rice University, Houston, Texas
Received July 14, 1964

Some things are hurrying into existence, and others are hurrying out of it;
and of that which is coming into existence part is already extinguished.
—MARCUS AURELIUS

ABSTRACT

Nucleosynthesis of elements heavier than the iron group by neutron capture on both slow and fast time scales is evaluated. The *s*-process calculations of Clayton, Fowler, Hull, and Zimmerman (1961) have been revised to include more recent experimental results on abundances and neutron capture cross-sections. The solar-system *s*-process abundances indicate a history of neutron exposure distributions characterized by decreasing probability of high integrated flux; an exponential exposure distribution is extracted. Estimates are made of the *s*-process contribution to each isotopic abundance; a table gives the amounts of elements produced by each process in the solar-system material. The *r*-process calculations are carried out using a semi-empirical atomic-mass law to determine neutron-binding energies and beta-decay probabilities. The solar-system *r*-process material has probably been synthesized in two distinct types of environments, e.g., one of about 4 sec duration with temperature $\sim 2.4 \times 10^9$ ° K and neutron density $\sim 5 \times 10^{26}$ cm^{-3}, and the other of the same or longer duration with temperature $\sim 1.0 \times 10^9$ ° K and neutron density $\sim 3 \times 10^{25}$ cm^{-3}; both of these environments could be found in an object with mass $\sim 10^5 M_\odot$.

I. INTRODUCTION

The purpose of this paper is to reappraise our understanding of the solar-system abundances of the heavy elements. The collective name *heavy elements* is used to designate elements more massive than those in the iron-group abundance peak. The first of the *heavy nuclear species* in the terminology employed here is thus Cu^{63}. This grouping is natural since the iron-peak elements represent the end product of energy-generating processes via charged-particle reactions (the *e*-process of Burbidge, Burbidge, Fowler, and Hoyle 1957), whereas the heavy elements are synthesized, in the main, only by chains of neutron capture on slow (*s*-process) and rapid (*r*-process) time scales. The relatively inefficient *p*-process of proton addition or photoneutron emission is ignored in this paper, since the level of abundances produced by that process is small in comparison to uncertainties in the *sr*-process abundances. Only in the neutron-poor species which are bypassed by both the *s*- and *r*-processes can the effects of the *p*-process be discerned. We choose to discuss *solar-system* abundances, since these are the abundances for which the observational evidence is most complete and detailed.

Our present concern with the synthesis of the heavy elements has been motivated by the following factors: (1) one of us (P. A. S.) has concluded his investigation of the systematics of nuclear binding energies central to the *r*-process theory; (2) H. C. Urey (1964) has recently summarized and interpreted the meteoric data on heavy-element abundances; (3) Macklin and Gibbons (1964) have presented the results of the Oak Ridge investigations of neutron-capture cross-sections pertinent to the *s*-process; (4) the solar-

* Supported in part by the Office of Naval Research and the National Aeronautics and Space Administration.

† Now at Los Alamos Scientific Laboratory, Los Alamos, New Mexico.

system σN-curve for the s-process differs noticeably from the earlier presentation of Clayton, Fowler, Hull, and Zimmerman (1961); and (5) many experimental r-process abundances may now be inferred from the differences between the observed abundances and the yield of the s-process.

The problem of understanding the abundances of the heavy elements involves a comparison or correlation of observational data (e.g., meteoric abundances) with calculations on the rates of nuclear processes under a variety of astrophysical or cosmological circumstances. These calculations must be based on experimental determinations of nuclear cross-sections and binding energies whenever possible. Normalization of the calculated values to the observational data is necessary because the calculations are incomplete—they yield only relative heavy-element abundances at best, and then only over limited ranges of atomic weight and atomic number. The normalizations of calculated abundance-curves are in reality measures of the efficiencies and frequencies of the stellar or cosmic events in which the nuclei were synthesized. In particular, the distribution of neutron fluxes for both the s- and r-processes is to be determined by normalization to the observed solar-system abundances. This technique was first applied by Clayton *et al.* (1961) to the s-process, but more recent data now require that their results be revised.

Whereas s-process calculations have been adequately treated by Clayton *et al.* (1961), r-process calculations have remained relatively intractable, and few conceptual advances have occurred since the original treatment of B^{2}FH (1957) and Becker and Fowler (1959). In this paper a semi-empirical mass law is used in the calculation of the shape of the r-process abundance distribution. The calculation depends on binding energies and beta-decay lifetimes for nuclei on the very neutron-rich side of the valley of beta-stability where nuclear properties cannot be experimentally determined and the accuracy of the extrapolation of the mass law is uncertain. We must, nonetheless, respond to the obligation of correlating the observational abundances with the most reasonable extrapolations of currently available nuclear measurements.

The outline of the paper is as follows. In the next section we choose the heavy-element abundances to be used to represent the solar system, in which choice we are guided by the review of Urey (1964). In Section III we review the status of the s-process contributions to solar-system material, based upon the methods of Clayton *et al.* (1961) and the recent review of neutron-capture cross-sections (Macklin and Gibbons 1964), and we extract an "experimental" r-process abundance-curve by subtracting the s-process contributions from the abundances given in Section II. In Section IV the various steps in the calculation of r-process abundances are described and carried out in detail. Finally in Section V conclusions are drawn concerning possible environments in which the r-process could have occurred, and some possible implications on galactic history.

II. THE ABUNDANCES OF THE ELEMENTS

The intent of this section is not that of adding a new abundance table to the literature. We maintain that element abundances should be determined by experimental research in geochemistry, geophysics, spectroscopy, and astrophysics. This attitude is logically necessary to avoid circularity in development of ideas concerning nucleosynthesis. We wish to evaluate quantitatively, however, the correlation between abundances and ideas of nucleosynthesis, and to do so requires a table of heavy-element abundances. This table must be based, so far as possible, on observation, supplemented by interpolations and extrapolations guided by ideas of nucleosynthesis only when absolutely necessary.

Advance in the knowledge of heavy-element abundances has been rapid in recent years. The meteoritic evidence reviewed by Suess and Urey (1956), which was largely chemical, has been augmented by the results of the technique of neutron activation. The large volume of new data acquired primarily by this technique has been summarized recently by Urey (1964). In this work Urey also reviews the modern ideas of chemical

fractionation as applied to the classes of meteorites, especially the ordinary, the enstatite, and the carbonaceous chondrites.

It has become increasingly apparent that the carbonaceous chondrites offer a more reliable sample of certain elements than do the ordinary chondrites, as pointed out by Reed, Kigoshi, and Turkevitch (1960). However, because of the variability of the sodium and potassium in carbonaceous chondrites, Urey has discarded his initial suggestion (Urey 1961) that these chondrites represent *as a class* primitive solar matter, although he has always thought the original material to be somewhat like the carbonaceous chondrites (Urey 1964). Ringwood (1961) has argued that one specific carbonaceous chondrite, orgueil, is a sample of primitive solar matter. However, Urey (1964) has warned that the iron abundance in carbonaceous chondrites is greater by a factor of 3 than the solar abundance of iron inferred from its spectral lines, and that the iron-cobalt ratio is markedly greater in all classes of chondrites than it is in the Sun. It seems that at present one cannot accept any single group of meteorites as representative of solar abundances. Faced with the necessity of making a choice, we have taken the ordinary chondrites as representative of the abundances of most elements, with the exceptions now to be discussed.

There is considerable evidence that the chalcophile elements have been depleted in ordinary chondrites. For those elements there is a good reason for choosing the carbonaceous chondrite abundances in preference to those of the ordinary chondrites. The most notable examples are indium, thallium, lead, and bismuth; lead and bismuth are known to be chalcophile, and it is a reasonable assumption that indium and thallium also have that character (Urey 1964). Selenium, tellurium, zinc, cadmium, mercury, and possibly iodine have known or inferred chalcophile characteristics that would make them likely candidates for depletion in ordinary chondrites by the same mechanism responsible for the low abundances of lead and bismuth. It will be noted that the carbonaceous chondrite abundances have been favored for these elements.

Table 1 lists the heavy-element abundances used in this paper. They have been chosen from the range of observed values reported by Urey (1964) on the basis of the above considerations. Further observational evidence is necessary. For complete references, see Urey (1964); other sources of information are also listed in the table. We must emphasize that the values given here are not definitive because of the arbitrary manner in which averages were taken, but that we believe these numbers represent a reasonable caricature of the abundance-curve. The remainder of the paper will be concerned with the implications of these abundances for ideas concerning nucleosynthesis.

The elements iron, cobalt, and nickel, excluded from Table 1, provide a different class of abundance problem, both experimentally and theoretically. Although they are synthesized primarily by a different process (*e*-process) than the heavy elements whose abundances constitute the main burden of this paper, they have significance as seed nuclei for the *s*- and *r*-processes. The *s*-process certainly has built upon seed-iron nuclei, and the *r*-process may have done so as well. The fraction of iron-group nuclei exposed to neutron fluxes of various intensities has important implications for nucleosynthesis and galactic history. One of the problems associated with this fraction and with a theory of meteorite formation is the discrepancy between the iron abundance in the Sun and in the various classes of meteorites, as shown in Table 2. (The Si = 10^6 scale is used in this paper.) One of the important remaining problems in cosmogonical science is the resolution of this discrepancy. The problem has been discussed in detail, particularly in regard to isotopic abundances of the *e*-process elements, by Fowler and Hoyle (1964).

III. THE *s*-PROCESS AND RELATIVE ABUNDANCES

Clayton *et al.* (1961) discussed the details of the *s*-process synthesis of the heavy elements. Those authors computed the distribution of the products of the neutron-capture cross-section times the abundances resulting from the exposure of Fe^{56} nuclei to a neutron

TABLE 1

ATOMIC ABUNDANCE PER 10^6 SI ATOMS

Element	Z	Abundance	Source
Cu	29	260	Average all Chondrites, Mason 1962
Zn	30	260	Average all Chondrites*
Ga	31	11.9	Chondrites
Ge	32	50	Average all Chondrites
As	33	4.6	Chondrites
Se	34	45	(2.5 × Chondrites)*
Br	35	13.4	Suess and Urey (1956)
Kr	36	30?	Interpolated
Rb	37	4.4	Chondrites
Sr	38	24	"
Y	39	4.7	"
Zr	40	16	" (Schmitt et al. 1964)
Nb	41	1.0	Suess and Urey (1956)
Mo	42	2.5	Chondrites
Ru	44	1.44	"
Rh	45	0.27	"
Pd	46	0.94	"
Ag	47	0.13	"
Cd	48	2.0	Enstatite and Carbonaceous Chondrites*
In	49	0.11	Suess and Urey (1956)
Sn	50	1.5	Enstatite and Carbonaceous Chondrites
Sb	51	0.15	Chondrites
Te	52	2.9	Enstatite and Carbonaceous Chondrites*
I	53	0.31	Enstatite and Carbonaceous Chondrites*
Xe	54	3.2?	Interpolated
Cs	55	0.22	Average all Chondrites
Ba	56	4.5	Average all Chondrites
La	57	0.39	Chondrites
Ce	58	1.17	"
Pr	59	0.14	"
Nd	60	0.64	"
Sm	62	0.23	"

TABLE 1 (continued)

Element	Z	Abundance	Source
Eu	63	0.082	Chondrites
Gd	64	0.34	"
Tb	65	0.051	"
Dy	66	0.33	"
Ho	67	0.076	"
Er	68	0.23	"
Tm	69	0.031	"
Yb	70	0.176	"
Lu	71	0.035	"
Hf	72	0.161	"
Ta	73	0.020	"
W	74	0.12	"
Re	75	0.054	Iron Meteorites (Herr et al. 1961)
Os	76	0.60	" " "
Ir	77	0.31	" " (Nichiporuk and Brown 1962)
Pt	78	0.89	" "
Au	79	0.13	Chondrites
Hg	80	0.15	Fitted to Pt via s-only isotopes
Tl	81	0.11	Enstatite and Carbonaceous Chondrites*
Pb	82	2.5	Sun (Helliwell 1961), Enstatite and Carbonaceous*
Bi	83	0.75	Fitted to Pb

* For all chalcophilic elements the enstatite and carbonaceous chondrites have been favored. This bias is most obvious in the case of Se, for which we use an abundance 2.5 times greater than that in the ordinary chondrites. We anticipate that Se will be considerably greater in Enstatite and Carbonaceous Chondrites than in ordinary Chondrites.

flux resulting in an average of n_c neutron captures per initial iron nucleus. They designated that $\sigma(A)N_s(A)$ product, when normalized to one initial Fe^{56} nucleus, by $\psi_A(n_c)$ or $\psi_A(\tau)$, where τ is the integrated product of neutron flux times time, in units of 10^{27} neutrons/cm^2. It was further argued that the product $\sigma(A)N_s(A)$ actually observed in the solar-system material should be a smooth curve representable in terms of a superposition of differing flux histories as

$$\sigma(A)N_s(A) = \int_0^\infty g(n_c)\psi_A(n_c)\,dn_c = \int_0^\infty \rho(\tau)\psi_A(\tau)\,d\tau\,, \qquad (1)$$

where $\rho(\tau)d\tau$ is the number of iron nuclei (per 10^6 Si atoms) exposed to integrated neutron fluxes between τ and $\tau + d\tau$, and $g(n_c)dn_c$ is the number of iron nuclei exposed to a neutron flux resulting in an average of n_c captures in the range dn_c. The subscript s on $N_s(A)$ accentuates the fact that only those abundances believed to be due to the s-process should be used in equation (1). The practical consequence of this restriction is

TABLE 2

IRON ABUNDANCE

Object	Atoms/10^6 Si	Reference
Chondrites, L-group	0.579×10^6	Urey 1964
Chondrites, H-group	$.799\times10^6$	Urey 1964
Enstatite chondrites	$.912\times10^6$	Urey 1964
Carbonaceous chondrites	$.833\times10^6$	Urey 1964
Weighted chondrite average	$.849\times10^6$	Mason 1962
Sun	$.12\times10^6$	Goldberg, Müller, and Aller 1960
Sun	0.12–0.20×10^6	Goldberg 1964

the limitation of the σN_s correlation to those nuclear species that (1) lie on the s-process path and are shielded from the r-process (s-only isotopes), or (2) lie on the s-process path and have r-process contributions that are small enough that they can be subtracted with reasonable confidence to obtain good estimates of the s-process abundances.

Once the σN_s-curve, which we shall hereafter call "$f(A)$," or the flux distribution $\rho(\tau)$ has been determined by fit to solar-system abundances, then N_s can be calculated for any isotope on the s-process path whose neutron-capture cross-section is known or can be estimated. The N_s can then be subtracted from observed abundances; the resulting "empirical" r-process curve will be discussed below.

a) The Solar-System σN_s-Curve

A hurdle to the implementation of s-process calculations has been the difficulty of measuring neutron-capture cross-sections for neutron energies in the range of a few tens of keV. Great progress has been made in that experimental art in the last few years, particularly by the physics division of Oak Ridge National Laboratory, whose efforts have resulted in a review of neutron-capture cross-sections pertinent to the s-process (Macklin and Gibbons 1964). They have averaged the cross-sections over a Maxwellian distribution of neutron energies. Their new report has been used in conjunction with the data listed by Clayton *et al.* (1961) to reconstruct $f(A) = \sigma N_s$ for solar-system abundances. Integrated cross-sections $\bar{\sigma}$ appropriate to $kT \approx 30$ keV are used, although the actual temperature of the s-process is still uncertain. The effects of temperature variation will be considered below; in general the effect on the calculations is small because most of the cross-sections vary in a similar manner with temperature.

The details of our correlation are shown in Table 3. The isotopic abundances are de-

TABLE 3

THE s-PROCESS σN CURVE

Species	Abundance	N_r (approx.)	N_s	$\bar{\sigma}$ (mb) kT = 30 keV	$\bar{\sigma} N_s$
Cu^{63}	179	0	179	64	1.15×10^4
Cu^{65}	81	0	81	24	1.95×10^3
Zn^{68}	48	0	48	30	1.44×10^3
Ge^{70}	10.3	s - only	10.3	100*	10^3
Ge^{74}	18.5	0	18.5	54	1.00×10^3
Se^{76}	4.1	s - only	4.1	150*	615
Kr^{82}	3.45?	s - only	3.45?	120*	415?
Sr^{86}	2.4	s - only	2.4	75	176
Sr^{87}	1.7	0.17†	1.5	108	163
Sr^{88}	20	1.0	19	6.9	130
Y^{89}	4.7	0.8	3.9	17	66
Zr^{90}	8.2	0.5	7.7	11	85
Zr^{92}	2.7	0.4	1.3	34	80
Zr^{94}	2.8	0.4	1.4	21	50
Mo^{96}	0.42	s - only	0.42	100*	47
Ru^{100}	0.18	s - only	0.18	300*	54
Pd^{104}	0.087	s - only	0.087	600*	52
Cd^{110}	0.25	s - only	0.25	300*	75
Sn^{116}	0.213	s - only	0.213	104	22
Te^{122}	0.073	s - only	0.073	--	--
Te^{123}	0.026	s - only	0.026	--	--
Te^{124}	0.136	s - only	0.136	200*	27
Xe^{128}	0.061	s - only	0.061	--	--
Xe^{130}	0.131	s - only	0.131	200*	26
Ba^{134}	0.108	s - only	0.108	--	--

TABLE 3 (continued)

Species	Abundance	N_r (approx.)	N_s	$\bar{\sigma}$ (mb) kT = 30 keV	$\bar{\sigma} N_s$
Ba^{136}	0.351	s - only	0.351	--	--
Ba^{138}	3.22	0.2	3.0	11	33
La^{139}	0.39	0.15	~ 0.24	45	~11
Nd^{142}	0.173	s - only	0.173	--	--
Sm^{148}	0.0272	s - only	0.0272	257	7.0
Sm^{150}	0.0170	s - only	0.0170	369	6.3
Gd^{154}	0.0075	s - only	0.0075	600*	4.5
Dy^{160}	0.0075	s - only	0.0075	800*	6.0
Yb^{170}	0.0053	s - only	0.0053	--	--
Hf^{176}	0.0083	s - only	0.0083	600*	5.0
Os^{186}	0.0096	s - only	0.0096	500*	4.9
Os^{187}	0.0099	0.006†	0.004	--	--
Pt^{192}	0.0069	s - only	0.0069	500*	3.5
Hg^{198}	0.0156	s - only	0.0156	250*	3.9
Pb^{204}	0.050	s - only	0.050	110	5.5
Pb^{206}	0.474	0.26‡	0.21	9.6	~2.0
Pb^{207}	0.516	0.38‡	0.14	8.7	~1.2

* Interpolated cross section

† Cosmoradiogenic decay of Rb^{87} and Re^{187} (Clayton 1964)

‡ Analysis of the r-process contributions to Pb^{206} and Pb^{207} is complicated, and proceeds along the lines of Clayton (1964). The preliminary values of $\bar{\sigma}(206)$ and $\bar{\sigma}(207)$ used there differ considerably from those used here, however, and Clayton's calculation must be restricted to high s-process temperatures (kT ≈ 60 keV), since the ratio $\sigma(206)/\sigma(207)$ now appears to be strongly dependent on kT. Quite tentative values are entered here for Pb^{206} and Pb^{207}, in order to demonstrate the likelihood that f(A) decreases in the lead isotopes.

rived from the elemental abundances of Table 1 and the isotopic fractions of Strominger, Hollander, and Seaborg (1958). All *s*-only isotopes are included in the table, as well as a number of isotopes produced also in the *r*-process, for most of which the correction is less than 20 per cent. For these the estimated N_r, or *r*-process contribution to the abundance, is given in the third column. Then N_s is found by subtraction. Some unmeasured cross-sections (denoted by an asterisk) for *s*-only species have been interpolated by us from nuclear systematics to give an additional guide to the outlines of $f(A)$, which is plotted in Figure 1.

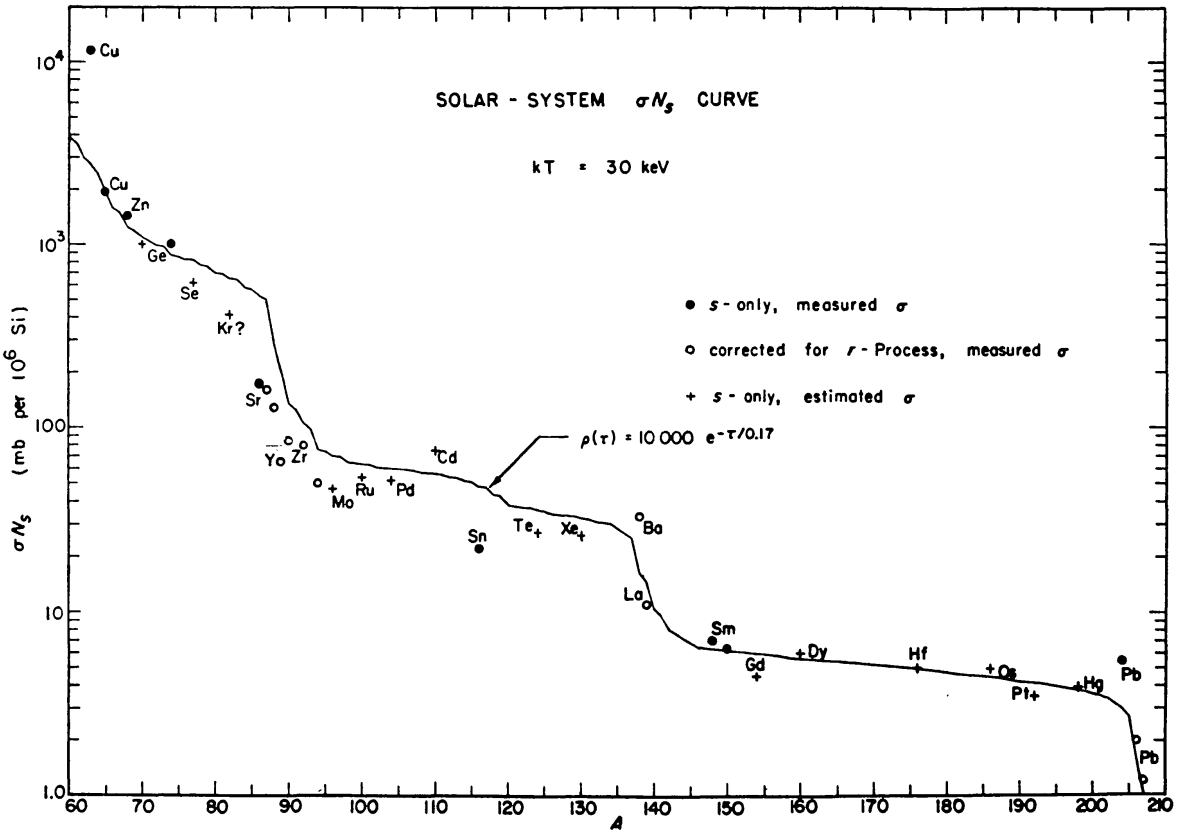

FIG. 1.—Solar-system σN_s-curve. The product of the neutron-capture cross-section at $kT = 30$ keV (in mb) times isotopic abundance (Si = 10^6) is plotted versus atomic mass number A. The solid line is a calculated curve corresponding to an exponential distribution of integrated neutron flux.

The points of Figure 1 show more structural detail than was apparent to Clayton *et al.* (1961). In particular, the relatively sudden decreases near $A = 88$–90 and $A = 138$–141 that were first suggested by those authors are now more evident. That this structure was anticipated as the likely result of the *s*-process provides further assurance of the correctness of the theory.

It should be noted that the points of Figure 1 can be adequately fit by a superposition of the form of Clayton *et al.* by the formula

$$f(A) = 2160\psi_A(n_c = 2.8) + 990\psi_A(n_c = 6.9) + 45\psi_A(n_c = 34) + 3.6\psi_A(n_c = 100)\ , \quad (2)$$

where only the final coefficient has been changed. However, the curve plotted in Figure 1 is *not* this type of discrete superposition; rather it is the result of a continuous distribution of exposures of the form

$$\rho(\tau) = Ge^{-\tau/\tau_0}\ . \quad (3)$$

Thus a surprisingly good fit has been obtained with a two-parameter curve, although such smooth distribution functions require a much more sudden drop from Sr to Zr than is apparent in the observations.

The functions $\psi_A(\tau)$ were calculated by equation (37) of Clayton *et al.* using the new cross-section data. The integral of equation (1) can be easily performed for exposure distributions of the form (3), yielding

$$f(A) = G\left(\frac{\lambda_A \tau_o}{\lambda_A \tau_o + 1}\right)^{m_A}, \tag{4}$$

where λ_A and m_A are given by equation (30) of Clayton *et al.* To check the accuracy of equation (4), we have computed $f(A)$ with the Bateman (exact) solution, also presented by Clayton *et al.*, and compared that solution to equation (4) for one choice of $\rho(\tau)$. The comparison showed that equation (4) is accurate enough for applied usage, and we have preferred it because of the decrease by a factor of almost 100 in the computer execution time.

The curve run through the points of Figure 1 was computed with $G = 10000$ and $\tau_o = 0.17$ for the cross-sections appropriate to $kT = 30$ keV. It appears that the essential feature of either a discrete or continuous exposure distribution is the rapidly diminishing probability of greater neutron exposures. This rapid decrease indicates that it may not be necessary in calculations of galactic history to demand that a single generation of stars be capable of producing large n_c values. That is, remixing into the second- and third-generation *s*-process events may be responsible for a significant fraction of the large neutron exposures. A quantitative calculation of this possibility is not warranted at present, but may ultimately provide clues to galactic evolution.

The cross-sections used in the curve in Figure 1 correspond to an *s*-process path passing through Sr^{86} (B^2FH); however, an alternative curve, based on an *s*-process path through Kr^{86} and on smaller assumed values for the Kr^{84} and Kr^{86} cross-sections as discussed in Section III*d*(i) below, is essentially identical with the curve shown. *Thus, if an exposure distribution of the form (3) is used,* the *s*-process is compatible only with high strontium and low zirconium abundances. Further understanding of these σN_s values is necessary.

Suffice it to say that the *s*-process calculations seem to be confirmed beyond any reasonable doubt and the general nature of the neutron exposure distributions revealed. The product σN_s for solar-system material is as shown in Figure 1. The demand that all *s*-process abundances fall on the curve will be of assistance in determining the semi-empirical *r*-process abundance-curve.

b) Other σN_s-Curves

One specific flux distribution was chosen to fit Figure 1. It is quite possible, however, that other stellar systems in our Galaxy, formed as they were at differing times and locations, may reveal flux histories different from that required to reproduce the solar-system abundances. There is, furthermore, no assurance that $kT = 30$ keV is a representative temperature for the *s*-process. Neutron-liberating reactions can occur for a wide range of temperatures. Since the averaged cross-sections will have different values at different temperatures, the neutron-flux distribution required to produce a given abundance distribution will also vary with temperature. Accordingly, we present at this point some more general examples of hypothetical *s*-process histories.

Exponential forms of $\rho(\tau)$ result from simple remixing models of the Galaxy for which the integrated flux τ is proportional to the number of times the seed have been processed through a stellar interior. Figures 2, 3, and 4 demonstrate families of $f(A)$ curves belonging to different values of τ_o. The curves of Figure 2 are computed with a value of $G = 10^4$ and with cross-sections appropriate to $kT = 15$ keV, whereas Figures 3 and 4 correspond respectively to $kT = 30$ keV and to $kT = 55$ keV. It is of interest to note that the shape

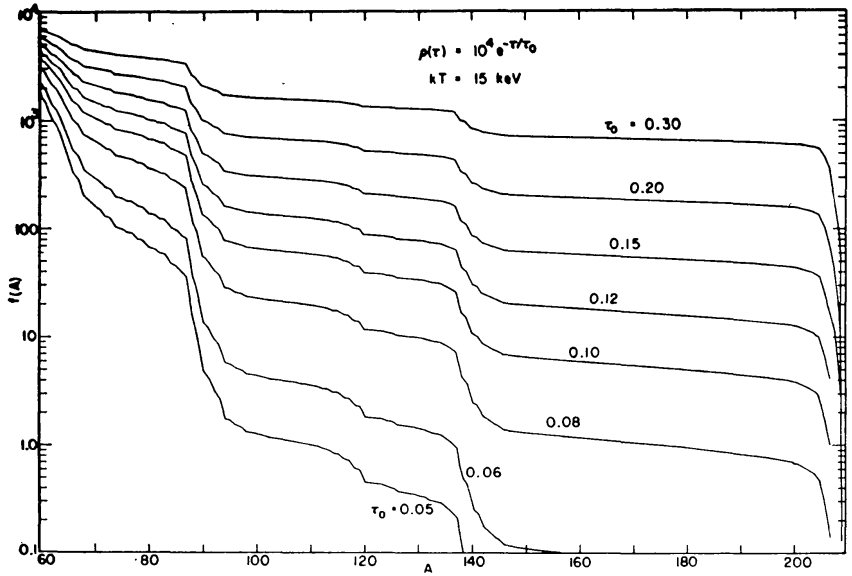

FIG. 2

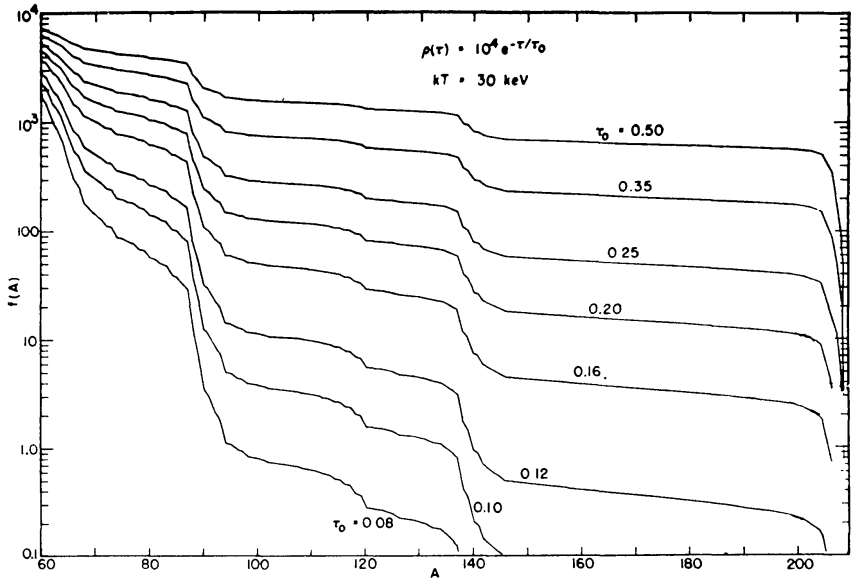

FIG. 3

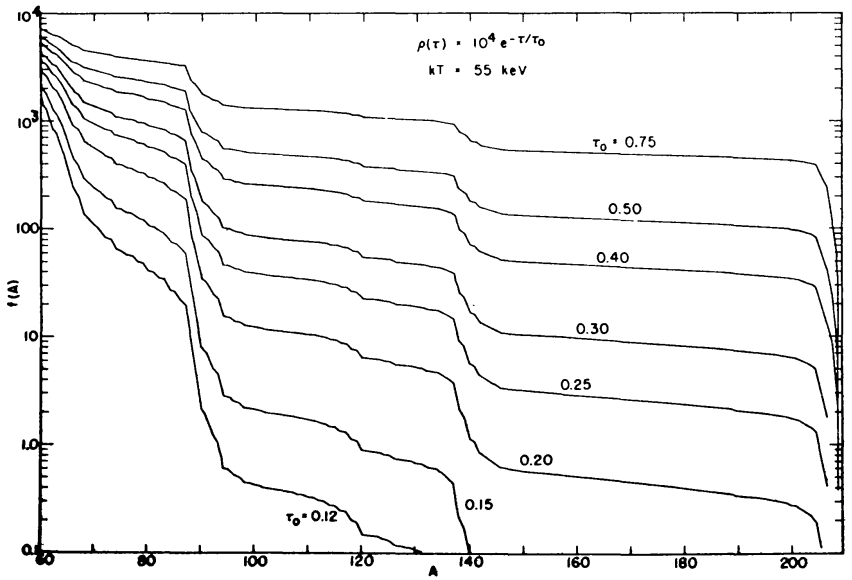

FIG. 4

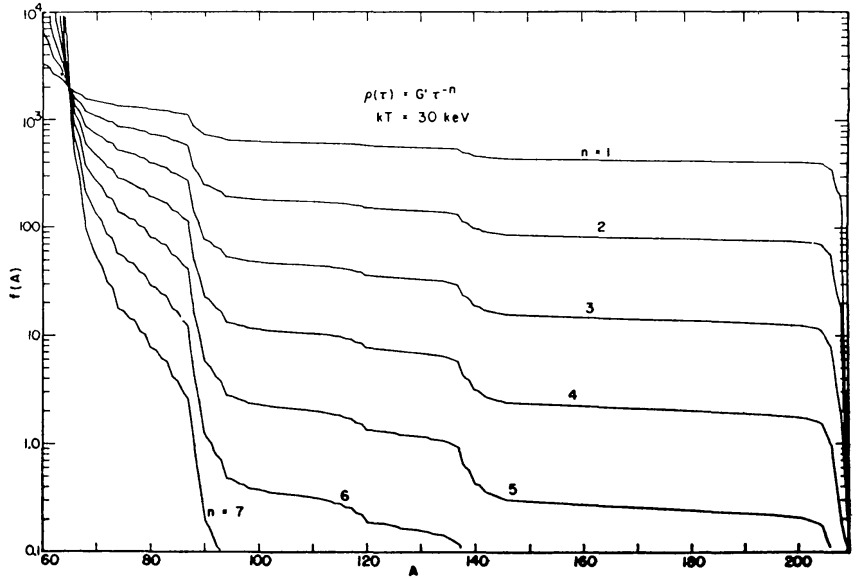

FIG. 5

FIGS. 2–5.—Calculated σN_s-curves. The results of calculations using cross-sections appropriate to kT = 15 keV, 30 keV, and 55 keV, respectively, are shown for various exponential distributions of integrated neutron flux.

of $f(A)$ for a given τ_0^{30} at 30 keV is nearly the same as that at 15 keV for $\tau_0^{15} = 0.60\ \tau_0^{30}$, a result of the fact that the cross-sections at 30 keV are characteristically about 60 per cent of their value at 15 keV. Similarly, the corresponding shape at 55 keV is given by the condition $\tau_0^{55} = 1.6\ \tau_0^{30}$. Thus the shape of a σN_s-curve cannot be expected to yield the temperature of the s-process, but it will give information about $\rho(\tau)$ when the temperature has been selected by another means. A word of caution must be inserted here, however. The *observed* σN_s-curves also depend upon the assumed temperature via the temperature dependence of the cross-sections. Thus the solar-system σN_s-curve, for instance, will be different at 15 keV or 55 keV than it is for the 30-keV cross-sections actually used in Figure 1. It would be an error to match the points of Figure 1 to one of the $f(A)$ curves of Figure 2 or Figure 4 without first replotting Figure 1 with cross-sections belonging to the appropriate temperature.

We wish to emphasize that the ledge-precipice structure of Figures 1–4 is not the result of special assumptions, but is rather the logical result of the most general assumption—that $\rho(\tau)$ is a smoothly decreasing function of τ. To illustrate this point, $f(A)$ has also been evaluated for power-law flux distributions,

$$\rho(\tau) = G'\tau^{-n} . \tag{5}$$

The integral of equation (1) may again be explicitly evaluated, using equation (37) of Clayton *et al.* (1961) for $\psi_A(\tau)$, yielding

$$f(A) = G'\lambda_A{}^n \frac{\Gamma(m_A - n)}{\Gamma(m_A)} . \tag{6}$$

A family of $f(A)$ curves for $kT = 30$ keV belonging to some integral values of the power-law exponent n is shown in Figure 5. Each curve has been normalized to have the same value at $A = 65$. Comparison with Figure 1 shows that no single index n yields as good a fit as the exponential families, but limited regions of A can be fit with values of n between about 2 and 4. Thus the solar-system σN_s-curve can be reproduced by a variety of discrete or continuous exposure distributions, which all have the common attribute of a rapidly decreasing probability of higher exposures. In particular, any monotonically decreasing distribution will produce the ledges as seen in Figures 1–5.

c) *Subtraction of* s-*Process Abundances*

All values of the product σN_s must fall on the curve $f(A)$. In particular, the s-process contribution to the abundances of those elements which are produced in both the s- and r-processes must be given by $N_s(A) = f(A)/\sigma(A)$. Then the abundance N_r due to the r-process may be found by subtraction. This subtraction must be performed to obtain the majority of the r-process abundances to be determined in this section. In this regard we must point out that most of the neutron-capture cross-sections have not been measured, but must be estimated from nuclear systematics. In that sense the present subtraction can by no means be considered definitive; these r-process abundances are presented as the best estimates that can be made at present. Subtraction is not always necessary, because there are many cases for which the nuclear abundance has received no significant contribution from the s-process. In such a case the total abundance is due to the r-process.

The table of r-process abundances begins at the first r-process peak with Ge^{76} (see Table 4). The first three columns of the table define the nuclear species and give its abundance. The fourth column, headed σ, gives the measured or estimated value of $\bar{\sigma}$ (in mb) corresponding to $kT = 30$ keV, or the comment "r-only" if the nuclide is bypassed in the s-process. Those cross-sections which are measured are given directly; those which are not measured are usually estimated as ratios, as in the case of the Se isotopes which are referred to $\sigma(76)$. The next column, $f(A)$, gives either the isotope whose

TABLE 4

THE r-PROCESS ABUNDANCES

A	Element	Abundance	σ (mb)	f(A)	N_s	N_r
76	Ge	3.8	r - only		0	3.8
77	Se	3.4	3.3 σ (76)	Se^{76}	1.2	2.2
78	Se	10.7	0.67σ (76)	Se^{76}	6.1	4.6
79	Br	6.8	2.2 σ (76)	Se^{76}	1.8	5.0
80	Se	22.5	0.5 σ (76)	Se^{76}	8.2	14.3
81	Br	6.6	2.2 σ (76)	Se^{76}	1.8	4.8
82	Se	4.0	r - only		0	4.0
83	Kr	3.45	2.5 σ (82)	Kr^{82}	1.38	2.07
84	Kr	17.1	0.5 σ (82)	Kr^{82}	6.9	10.2 ‡
			0.25σ (82)	Kr^{82}	13.8	3.3 ‡
85	Rb	3.2	181	?		?
86	Kr	5.2	r - only		0	5.2 ‡
			0.10σ (82)	Kr^{82}	~3?	~2 ‡
87	Rb	1.2	r - only		0	1.37*
88	Sr	20	6.9	0.75 Sr^{86}	19 ?	? †
89	Y	4.7	17	100	6 ?	? †
90	Zr	8.2	11	90	8.2	? †
91	Zr	1.8	59	80	1.4	0.4
92	Zr	2.7	34	70	2.1	0.6
93	Nb	1.00	264	60	0.23	0.77
94	Zr	2.8	21	50	2.4	?
95	Mo	0.40	2.5 σ (98)	Mo^{96}	0.17	0.23
96	Zr	0.45	r - only?		0?	≲0.45
97	Mo	0.24	2.5 σ (98)	Mo^{96}	0.17	0.07
98	Mo	0.61	102	Mo^{96}	0.42	0.19

TABLE 4 (continued)

A	Element	Abundance	σ (mb)	f(A)	N_s	N_r
99	Ru	0.185	3.3 σ (100)	Ru^{100}	0.055	0.13
100	Mo	.24	r - only		0	0.24
101	Ru	.245	2.5 σ (100)	Ru^{100}	0.073	0.17
102	Ru	.452	0.67σ (100)	Ru^{100}	0.27	0.18
103	Rh	.27	3.3 σ (100)	Ru^{100}	0.05	0.22
104	Ru	.264	r - only		0	0.264
105	Pd	.214	3 σ (104)	Pd^{104}	0.03	0.18
106	Pd	.255	0.67σ (104)	Pd^{104}	0.13	0.13
107	Ag	.067	~1000	45	0.045	0.02
108	Pd	.251	0.5 σ (104)	Pd^{104}	0.17	0.08
109	Ag	.063	~1000	45	0.045	0.02
110	Pd	.127	r - only		0	0.127
111	Cd	.256	2.5 σ (110)	Cd^{110}	0.10	0.16
112	Cd	.476	0.67σ (110)	Cd^{110}	0.375	0.10
113	Cd	.248	1.67σ (110)	Cd^{110}	0.15	0.10
114	Cd	.576	0.5 σ (110)	Cd^{110}	0.50	?
115	In	.11	~1000	40	0.04	0.07
116	Cd	.152	r - only		0	0.152
117	Sn	.115	418	Sn^{116}	0.053	0.06
118	Sn	.358	65	Sn^{116}	0.338	? †
119	Sn	.132	257	Sn^{116}	0.086	0.05
120	Sn	.490	41	Sn^{116}	0.53	? †
121	Sb	.086	~500	Sn^{116}	0.04	0.05
122	Sn	0.071	r - only		0	0.071

TABLE 4 (continued)

A	Element	Abundance	σ (mb)	f(A)	N_s	N_r
123	Sb	0.064	r - only		0	0.064
124	Sn	0.089	r - only		0	0.089
125	Te	0.203	2.5 σ (124)	Te^{124}	0.045	0.16
126	Te	0.543	0.67σ (124)	Te^{124}	0.20	0.34
127	I	0.31	737	25	0.03	0.28
128	Te	0.920	r - only		0	0.920
129	Xe	0.842	2.5 σ (128)	Xe^{128}	0.024	0.82
130	Te	0.995	r - only		0	0.995
131	Xe	0.683	1.67σ (128)	Xe^{128}	0.036	0.65
132	Xe	0.865	0.67σ (130)	Xe^{130}	0.20	0.66
133	Cs	0.22	462	22	0.05	0.17
134	Xe	0.336	r - only		0	0.336
135	Ba	0.296	1.5 σ (134)	Ba^{134}	0.072	0.22
136	Xe	0.288	r - only		0	0.288
137	Ba	0.508	1.5 σ (136)	Ba^{136}	0.24	0.27
138	Ba	3.22	11.4	?		? †
139	La	0.39	45	10	0.22	0.17
140	Ce	1.02				? †
141	Pr	0.14	95	8	0.08	0.06
142	Ce	0.13	r - only		0	0.13
143	Nd	0.078				?
144	Nd	0.153				?
145	Nd	0.053				?
146	Nd	0.110				?

TABLE 4 (continued)

A	Element	Abundance	σ (mb)	f(A)	N_s	N_r
147	Sm	0.0362	1169	7.0	0.0060	0.0302
148	Nd	.036	r - only		0	.036
149	Sm	.0334	1617	6.8	0.0042	.0292
150	Nd	.036	r - only		0	.036
151	Eu	.039			0.004	.035
152	Sm	.0636	410	6.0	0.0146	.049
153	Eu	.043	~2000	6	0.003	.040
154	Sm	.0543	r - only		0	.0543
155	Gd	.0504	2.5 σ (154)	Gd^{154}	0.003	.047
156	Gd	.0702	0.67σ (154)	Gd^{154}	0.011	.059
157	Gd	.0531	1.67σ (154)	Gd^{154}	0.004	.049
158	Gd	.0840	0.44σ (154)	Gd^{154}	0.016	.068
159	Tb	.051	1908	6	0.003	.048
160	Gd	.0742	r - only		0	.0742
161	Dy	.0625	2.5 σ (160)	Dy^{160}	0.003	.060
162	Dy	.0844	0.67σ (160)	Dy^{160}	0.011	.073
163	Dy	.0826	1.67σ (160)	Dy^{160}	0.004	.079
164	Dy	.0932	0.44σ (160)	Dy^{160}	0.016	.077
165	Ho	.076	1792	6	0.003	.073
166	Er	.076			0.008	.068
167	Er	.056	~2000	6	0.003	.053
168	Er	.060			0.012	.048
169	Tm	.031	1298	6	0.005	.026
170	Er	0.032	r - only		0	0.032

TABLE 4 (continued)

A	Element	Abundance	σ (mb)	f(A)	N_s	N_r
171	Yb	0.025	2.5 σ (170)	Yb^{170}	0.002	0.023
172	Yb	.038	0.67σ (170)	Yb^{170}	0.008	.030
173	Yb	.029	1.67σ (170)	Yb^{170}	0.003	.026
174	Yb	.054	0.44σ (170)	Yb^{170}	0.012	.042
175	Lu	.034	1623	6	0.004	.031
176	Yb	.022	r - only		0	.022
177	Hf	.0295	2.5 σ (176)	Hf^{176}	0.003	.027
178	Hf	.0436	0.67σ (176)	Hf^{176}	0.012	.032
179	Hf	.0221	1.67σ (176)	Hf^{176}	0.005	.017
180	Hf	.0567	~300	6	0.020	.037
181	Ta	.020	760	6	0.008	.012
182	W	.032			0.012	.020
183	W	.017			0.005	.012
184	W	.037	350	6	0.017	.020
185	Re	.020	~2000	6	0.003	.017
186	W	.034	r - only		0	.034
187	Re	.034	r - only		0	.040*
188	Os	.080	0.67σ (186)	Os^{186}	0.014	.066
189	Os	.097	1.67σ (186)	Os^{186}	0.006	.091
190	Os	.168	0.44σ (186)	Os^{186}	0.021	.147
191	Ir	.120	~800	6	0.008	.112
192	Os	.246	r - only		0	.246
193	Ir	0.190	~800	6	0.008	0.182

TABLE 4 (continued)

A	Element	Abundance	σ (mb)	f(A)	N_s	N_r
194	Pt	0.292	0.67σ (192)	Pt^{192}	0.010	0.282
195	Pt	.300	1.67σ (192)	Pt^{192}	0.004	0.296
196	Pt	.226	0.44σ (192)	Pt^{192}	0.015	0.211
197	Au	.13	605	6	0.010	0.12
198	Pt	.064	r - only		0	0.064
199	Hg	.0254	2.5 σ (198)	Hg^{198}	0.006	0.019
200	Hg	.0346	0.67σ (198)	Hg^{198}	0.024	0.011
201	Hg	.0198	1.67σ (198)	Hg^{198}	0.009	0.011
202	Hg	.0446	0.44σ (198)	Hg^{198}	0.036	0.009
203	Tl	.032			?	?
204	Hg	.0102	r - only		0	0.0102
205	Tl	0.078			?	?

‡ See discussion of Se-Kr peak.

* Cosmoradiogenic decay of Rb^{87} and Re^{187} have decreased the observed abundances of these isotopes by certain amounts, which have been added to obtain the values shown (Clayton 1964).

† These isotopes are dominated by the s-process to such an extent that determination of N_r by subtraction is impossible.

abundance N_s from Table 3 is used in the ratios, or the value of $f(A)$ estimated from Figure 1. The sixth column lists N_s, the contribution of the *s*-process to that species. Whenever the abundance of species A is referred to an *s*-only nucleus, its value was obtained by $N_s(A) = [\sigma(A')/\sigma(A)]N_{s\text{-only}}(A')$. (For *s*-only isotopes, refer to Table 3.) The final column shows the value of N_r obtained as the difference of the third and the sixth columns.

d) The r*-Process Abundances*

The values of N_r listed in Table 4 have been plotted against atomic weight in Figure 6, in which we have differentiated between four different types of data points on the basis of the relative size of the *s*-process subtraction. No point is plotted for which N_r is less than 20 per cent of the total isotopic abundance, resulting in numerous gaps in Figure 6. Isotopes of the same element are connected in the figure to illustrate the fact that changes in the *elemental* abundances cannot in general change the major features, which are outlined by the experimentally better-known isotopic ratios.

The gaps represent *r*-process abundances which are such a small fraction of the total that they cannot be obtained as a subtraction of the type performed in Table 4. It is clear, however, that the *r*-process curve of Figure 6 drops smoothly from its value at Rb to its value at Mo, passing through unity near $A = 90$. The gap there (and at $A = 140$) in Figure 6 does not imply that the general feature of the region is unknown, but rather that the specific values of the abundances cannot be meaningfully obtained by subtraction. The outstanding features of this curve that led B^{2}FH to their original formulation of the *r*-process are immediately evident: the abundance peaks at $A = 80$, 130, and 195. There can be little doubt about the existence of these peaks, although their detailed structure and size may yet be considerably in error. Because of the importance of these peaks, we wish to mention briefly some of the major problems associated with their determination.

i) *The Se-Kr peak.*—The first peak in Figure 6 shows a curious double structure that will, if it is due to the *r*-process, indicate some important properties of that process. As we will show, however, the second bump of the pair (Kr) may not be due to the *r*-process at all. The shape of the first peak at Se is set, within limits, by the abundance distribution of the selenium isotopes. A measurement of the isotopic neutron-capture cross-sections of Se would allow unequivocal determination of its shape by securing the *s*-process subtraction. The absolute size of the peak depends on the Se abundance, for which a value 2.5 times the abundance in ordinary chondrites has been taken. Our enhancement of Se is based upon an assumed chalcophile character, an uncertainty that may be resolved by measurement of the Se concentration in carbonaceous chondrites. The values of Br^{79} and Br^{81}, uncertain as the Br abundance is, fit reasonably well into the Se peak.

The second peak in the pair (at Kr^{84}) results from adhering to the original *s*-process path of B^{2}FH (1957). Those authors assumed that neutron-capture times were of the order of 10^4 years, which, if true, implies that the *s*-process path changes Z when it passes through a beta-decay lifetime short compared to 10^4 years. In particular, they assumed that Kr^{85}, with $\tau(\beta^-) = 10.3$ years, decays before capturing a neutron. Evidence tending to support their assumption is provided by the fact that Sr^{86} would be bypassed by both the *s*- and *r*-processes if Kr^{85} captures neutrons before decaying, whereas Sr^{86} seems to be in *s*-process equilibrium (compare to Sr^{87}, Table 3). And finally, the isotopic composition of Kr seems in itself to indicate large *r*-process contributions to both Kr^{84} and Kr^{86}. We have presented this B^{2}FH interpretation as one alternative in the construction of Table 4 and Figure 6, but we wish to consider also an alternative situation that would attribute the Kr peak to the *s*-process.

Since the $N = 50$ neutron shell closes at Kr^{86}, that nucleus will have a relatively small neutron-capture cross-section. Based on the values of the cross-sections of Sr^{88} and Zr^{90}, two similar $N = 50$ nuclei, we anticipate a value $\bar{\sigma}(Kr^{86}) \approx 12$ mb at $kT = 30$ keV. Since $\bar{\sigma}(Kr^{86})$ is about a factor of 10 smaller than $\bar{\sigma}(Kr^{82})$, it is apparent that the Kr^{86}

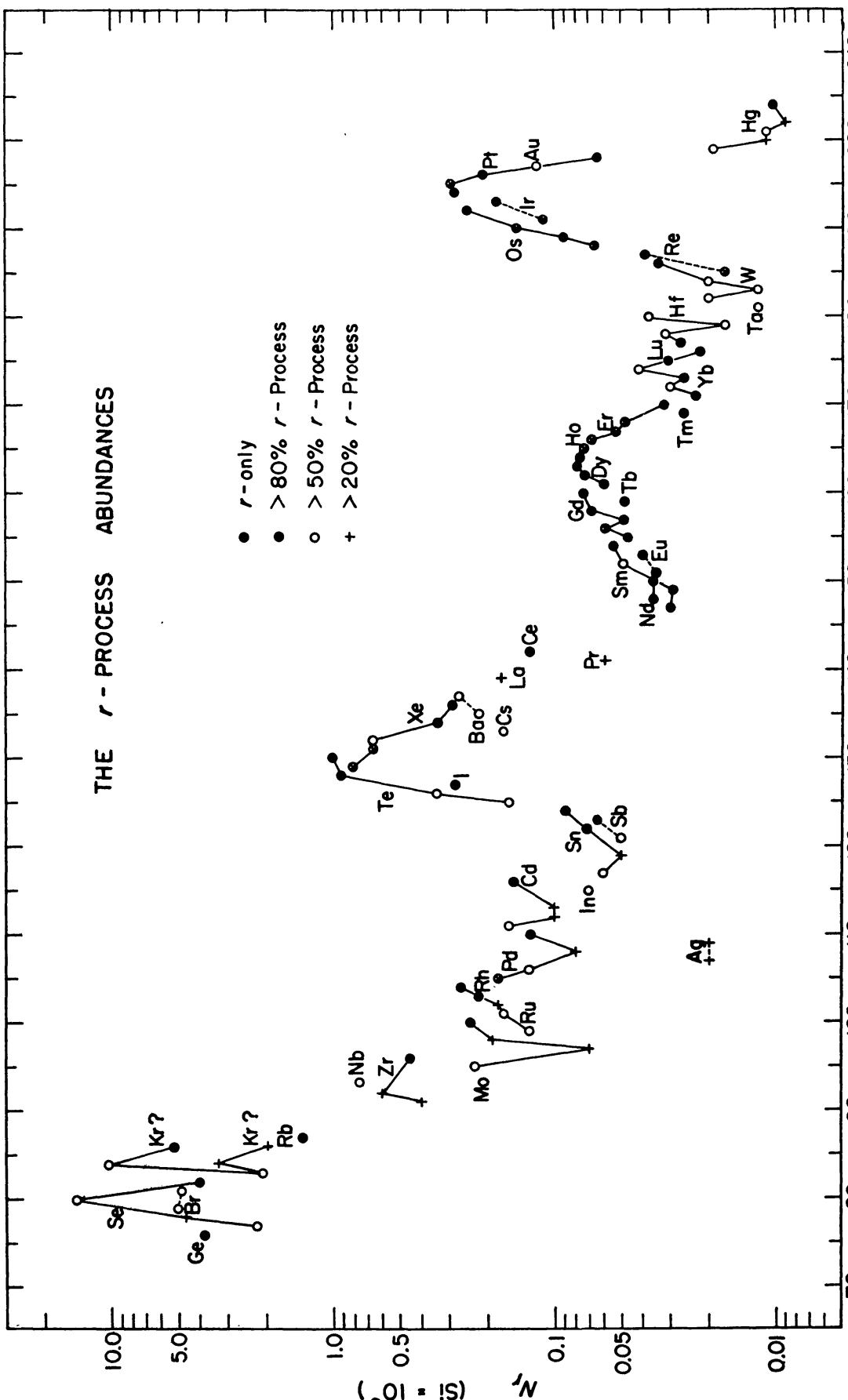

FIG. 6.—Solar-system *r*-process abundances. Abundances of isotopes produced in the *r*-process are plotted after subtraction of the contribution by the *s*-process. Isotopes of a given element are joined by lines (solid line = even *Z*, dashed line = odd *Z*). The ambiguity at Kr is discussed in the text.

abundance would have been about a factor of 10 greater than the abundance of Kr^{82} *if* Kr^{86} *lay on the* s-*process path;* i.e., if Kr^{85} captured neutrons faster than its 10.3-year beta-decay to Rb^{85}. Since the abundance $Kr^{86} = 5.2$ is of the same order as $Kr^{82} = 3.45$ (both based on Kr = 30), it is clear that Kr^{85} captured neutrons at a much slower rate than the beta-decay rate. How much slower, however, is not certain, because the time scale for the *s*-process has never been unambiguously determined. It is certainly possible that something of the order of 10 per cent of the Kr^{85} nuclei capture neutrons before beta-decay, in which case the *s*-process abundance of Kr^{86} is approximately equal to the abundance of Kr^{82}. We have entered this possibility as a second alternative for Kr^{86} in Table 4. Since this possibility requires a neutron-capture lifetime of about 100 years for Kr^{85}, it is of interest to see what the implications of such a lifetime would be on the branch at Se^{79} studied by B²FH.

It was pointed out by B²FH (p. 558) that Kr^{80} resulted from an *s*-process branch by which Se^{79} undergoes beta-decay before capturing a neutron. Those authors further showed that the ratio of half-lives must be $\tau_\beta(Se^{79})/\tau_n(Se^{79}) = 1.37$ in order to account for the Kr^{80} abundance. If Kr^{85} is to have a half-life against neutron capture of about 100 years, the corresponding half-life of Se^{79} should be about $\tau_n(Se^{79}) \approx 25$ years based upon a cross-section ratio (unmeasured) $\sigma(Se^{79})/\sigma(Kr^{85}) = 4$. The Kr^{80} abundance then demands $\tau_\beta(Se^{79}) = 1.37 \times 25 = 34$ years for the Se^{79} half-life, which is measured in the laboratory to be equal to 6.5×10^4 years. The discrepancy is easily accounted for by the fact that thermally populated excited states of Se^{79} speed up its beta-decay rate. Bahcall (1962) has calculated

$$\tau_{1/2}(Se^{79}) = \frac{6.5 \times 10^4 \text{ yr}}{1 + 6.47 \times 10^5 \exp(-11.1/T_8)}. \quad (7)$$

If equation (7) is to be equal to 34 years (within a factor of 3), the temperature must equal $T = 2.0 \pm 0.4 \times 10^8$ ° K. Since that temperature is close to the one at which neutrons will be rapidly released by the reaction $Ne^{22}(\alpha, n)Mg^{25}$ in helium-burning shells of giant stars, the plausibility of this time scale is enhanced. A neutron-capture time of 100 years for Kr^{85} implies times of 10^3–10^4 years for the complete chain.

The largest abundance in the possible *r*-process peak at krypton is due to the high abundance of Kr^{84}. The cross-section for Kr^{84} is just as likely to be 0.25 $\sigma(82)$ as 0.5 $\sigma(82)$, however, in which case Kr^{84} is also largely due to the *s*-process. This possibility has been entered as the second alternative for Kr^{84} in Table 4. In short we will summarize by asserting that the abundance peak at Kr may be attributable either to the *r*-process or to the *s*-process. The assignment cannot be made on the basis of present experimental evidence (see also Sec. V*a*[i] below). We urge that some technique be devised for measuring the neutron-capture cross-sections of the isotopes of Kr. Not only will such measurements settle this very interesting Kr problem, but the very uncertain elemental Kr abundance may be interpolated with greater confidence than at present if $\sigma(82)$ is known (see Table 3). Measurement of the cross-section of Kr^{80} will also be helpful in the establishment of the capture time scale by the technique involving the branch at Se^{79}.

ii) *The Te-Xe peak.*—This *r*-process peak is obvious simply from the isotopic compositions of Te and Xe; the absolute abundances are needed only to determine the height of the peak. The adopted abundance of Te = 2.9 should be quite good, although we have discarded the abundance measurements in ordinary chondrites as being deceptively low due to an assumed chalcophile character for Te. The abundance Xe = 3.2 was fitted to Te and Ba. In this regard we would like to suggest that measurements of the neutron-capture cross-sections of Xe^{128} and Xe^{130}, *s*-only isotopes, will provide the most unambiguous determination of the important xenon abundance.

iii) *The Os-Ir-Pt peak.*—The abundances in this peak appear to be on a firmer basis than those in the other two major *r*-peaks. The abundance in iron meteorites agrees well with the abundances in ordinary chondrites. The major uncertainty involved relates

to the fact that these siderophile elements may, if they have not been fractionated previously from iron, possess the same type of solar-meteoric discrepancy as iron. The meteoric iron abundances listed in Table 2 are two to seven times larger than the solar abundances. But even if the Os and Pt abundances used here are several times too large, there still exists a peak near $A = 194$.

We have not estimated the r-process contributions to Pb and Bi. This very complicated subject has been thoroughly discussed recently by one of us (Clayton 1964), and already the situation has been complicated by more detailed evaluation of the neutron-capture cross-sections of the lead isotopes (Macklin and Gibbons 1964). For this paper we will terminate the empirical r-process abundances at Hg.

e) Relative Source of Element Abundances

It has become important in astronomical studies of stellar evolution to differentiate between the processes of nucleosynthesis. Often such studies proceed by a comparison of the abundances observed in some star with the abundances of the same elements in the Sun. As an example, the s-process overabundances in barium stars have been determined in this manner (Burbidge and Burbidge 1957; Warner 1964). The interpretation of such a comparison in terms of nucleosynthesis mechanisms demands, however, that the relative contributions of the s- and r-processes to each element of solar-system material be clearly understood. Much of the new abundance and cross-section data has forced changes in the earlier estimates of Clayton *et al.* (1961, p. 405). For these reasons, the current evaluation of the sources of solar-system abundances is presented in Table 5. It is perhaps worth re-emphasizing that the solar-system partition between s- and r-process is the result of a specific history, and the relative contributions at another space time point in the Galaxy are not expected to be the same.

IV. CALCULATION OF r-PROCESS ABUNDANCES

To understand the existence of abundance peaks at $A = 80$, 130, and 195 in terms of nuclear shell structure requires an environment characterized by a high neutron density at a high temperature, e.g., $n_n = 10^{24}$ cm^{-3} and $T = 10^9$ ° K. Under such conditions neutron captures will be very rapid, and if the inverse (γ, n) reactions are also rapid compared to beta-decay, a situation very close to thermal equilibrium will be established between the isotopes of any element, neutrons, and photons. The calculations have been carried out assuming iron-group nuclei produced by other processes, e.g., the e-process, as the seed nuclei. The choice of iron seems a logical one, since it has an abundance about four orders of magnitude greater than the abundances of the heavier species to be produced by neutron capture (but see Sec. V*b*). The relative isotopic abundances of elements higher in Z than the seed will be independent of this choice. (The time scales calculated assuming initial iron nuclei would need to be lengthened only slightly for a starting point of lower Z.) Since the normal stable isotopes of iron ($Z = 26$) have small (γ, n) rates, they will be rapidly and irrevocably consumed by neutron capture, and the isotopes formed at equilibrium will be very neutron-rich. These will eventually ($t_{1/2} \sim 0.1$ sec) beta-decay to cobalt, the rate being slow enough not to affect the equilibrium distribution of the iron isotopes appreciably. Then an independent equilibrium will be established for cobalt isotopes ($Z = 27$), and so forth.

The relative abundances of the isotopes of each element depend on their nuclear properties and are functions only of the temperature and neutron flux under the ambient conditions at which the r-process occurs. On the other hand, at any given time, the relative amount of material at a given Z depends only on the relative beta-decay probabilities at each Z. If the neutron flux and temperature are suddenly turned off at some time (typically some seconds) after being turned on, the super-n-uated nuclei then in existence will beta-decay to stable isotopes. The effect of reactions other than beta-decay which occur during the cooling period cannot be computed at this time. However, the short time

TABLE 5

ELEMENTAL s- AND r-PROCESS ABUNDANCES

Element	Z	$N_s(Z)$	$N_r(Z)$	Element	Z	$N_s(Z)$	$N_r(Z)$
Se	34	19.6	25.1	Ce	58	0.9	0.2
Br	35	3.6	9.8	Pr	59	.08	.06
Kr	36	23(?)	7(?)	Nd	60	.4	.2
Rb	37	2.2	2.4	Sm	62	.069	.163
Sr	38	23	1	Eu	63	.007	.075
Y	39	3.9	0.8	Gd	64	.04	.30
Zr	40	13.8	2.2	Tb	65	.003	.048
Nb	41	0.3	0.7	Dy	66	.04	.29
Mo	42	1.2	0.7	Ho	67	.003	.073
Ru	44	0.74	0.58	Er	68	.02	.20
Rh	45	0.05	0.22	Tm	69	.005	.026
Pd	46	0.52	0.42	Yb	70	.03	.14
Ag	47	0.09	0.04	Lu	71	.004	.031
Cd	48	0.59	1.38	Hf	72	.05	.11
In	49	0.04	0.07	Ta	73	.008	.012
Sn	50	1.13	0.34	W	74	.034	.086
Sb	51	0.04	0.11	Re	75	.003	.057
Te	52	0.48	2.42	Os	76	.055	.55
I	53	0.03	0.28	Ir	77	.016	.29
Xe	54	0.45	2.75	Pt	78	.036	.85
Cs	55	0.05	0.17	Au	79	.010	.12
Ba	56	3.8	0.7	Hg	80	0.09	0.06
La	57	0.22	0.17				

scales which will be found imply a rapid decrease in the neutron density and corresponding increase in heavy-element abundances. Thus it may be that, even while the neutron density remains fairly high, the number of free neutrons per heavy nucleus may be so low that any changes in the abundance distribution during cooling would be slight.

Thus the r-process produces one isotope for each value of A, and the relative abundance at each A can be found by summing over each Z which has an isotope of that A among the progenitors. These abundances are then functions of three parameters (in addition to nuclear properties): neutron flux, temperature, and the duration of the process. The parameters are to be chosen which best reproduce the experimental data of Figure 6. Ultimately, of course, the physical conditions must be identified with a naturally occuring astrophysical situation.

The problem separates into four parts: (1) determination of nuclear binding energies for very neutron-rich nuclear species; (2) calculation of equilibrium for each element with charge number Z, giving relative isotopic distribution among progenitors; (3) calculation of beta-decay probability for each isotope and hence for each element; and (4) solution of the time-dependent problem for the relative amount of each element and thus for the relative abundance at each mass number, A.

a) Nuclear Binding Energies

To calculate the (n, γ) thermal equilibrium and to estimate beta-decay half-lives it is necessary to know binding energy differences between neighboring nuclei in the Z–A-plane. Such a complete knowledge of binding energies requires the use of a semi-empirical mass law. The problem of finding a mass law which can be extrapolated into the neutron-rich region with confidence has not been completely solved. The standard Bethe-Weizsäcker mass law is insufficient, but only the most prominent additional features of the mass surface need to be included in order to calculate the major features of the r-process. For instance, it is only necessary to account for "magic number" shell structure in the mass law in order to reproduce the three major peaks of Figure 6. Such a mass law is shown as the third column in Table 6, in which shell effects are represented by a parabolic term between each pair of magic numbers. To account for the broad maximum around $A = 164$ it is necessary to include adequate expressions for deformation energy in the mass law. The sixth column in Table 6 is an attempt to do this, using the Nilsson model to calculate deformations. In order to reproduce the r-process abundances in detail, however, it is necessary to have a mass law more accurate than any which can be envisioned at present. The basic difficulty lies in the fact that the mass law is fitted to nuclei near the bottom of the mass valley, whereas it is the properties of nuclei far up the neutron-rich side which are required. A form of the mass law which adequately describes nuclei deep in the mass valley may not be suitable for the more exotic species of present interest.

i) *Standard mass law.*—The form taken here for the standard mass law (Bethe and Bacher 1935; Seeger 1961) gives the binding energy $B(Z, A)$ as

$$B_o(Z, A) = \left(\alpha - \frac{\gamma}{A^{1/3}}\right) A - \left(\beta - \frac{\eta}{A^{1/3}}\right) \frac{I^2 + 4|I|}{A} + \delta\left(\pm \frac{1}{A^{1/2}}, 0\right) - 0.800 \frac{Z^2}{A^{1/3}} \left(1 - \frac{0.76361}{Z^{2/3}}\right)\left(1 - \frac{1.9605}{A^{2/3}}\right), \quad (8)$$

the "δ" term being positive for even-even nuclei, 0 for odd A, and negative for odd-odd nuclei. I is equal to $N - Z$.

The five parameters α, β, γ, η, and δ were found by least-squares fitting to the binding energies in the 1961 Mass Table (König, Mattauch, and Wapstra 1962). All nuclei with

both N and Z greater than or equal to 20 were used (825 data), and all were weighted equally. The results are given in the first column of Table 6. Since this mass law does not reproduce the abundance peaks, new physical terms must be added.

ii) *Inclusion of shell effects.*—The effects of shell structure are represented by adding a term between each pair of magic numbers in Z and N, which is quadratic and has a value 0 at each end of the shell. The coefficients are allowed to be different in each shell, but are the same for protons and neutrons. Thus

$$B_s(Z, A) = B_o(Z, A) - \zeta_j \frac{(N_{j+1} - N)(N - N_j)}{(N_{j+1} - N_j)^2} - \zeta_k \frac{(Z_{k+1} - Z)(Z - Z_k)}{(Z_{k+1} - Z_k)^2}, \quad (9)$$

where $N_j \leq N < N_{j+1}$ and $Z_k \leq Z < Z_{k+1}$, and the magic numbers are $Z_1 = N_1 = 20$, $Z_2 = N_2 = 28$, $Z_3 = N_3 = 50$, $Z_4 = N_4 = 82$, $Z_5 = N_5 = 126$, and $N_6 = 184$. The coefficients ζ are shown in the second column of Table 6 for a mass-law fit to all 825 data.

Since the shell and deformation terms are strongly correlated, especially in the higher shells, an additional mass law was calculated omitting data for nuclei expected to be deformed. The fourth column of Table 6 gives the results of a fit to 572 data, omitting all A in the ranges $150 \leq A \leq 190$ and $220 \leq A$; note that in the highest shells there are significant differences between the fourth column and the second column.

As neither of these adjustments was thought to give an adequate expression of the shell effects because of interference of deformations, three empirical terms suggested by Kümmel, Mattauch, Thiele, and Wapstra (1964) were included in an additional adjustment to all data, given in the third column. These extra terms, which act only in particular shells, allow a greatly improved fit to the masses along the line of beta stability. The mass law becomes

$$B_K(Z, A) = B_S(Z, A) + \delta_{j,4} \frac{(126 - N)(N - 82)}{(126 - 82)^2} \left[\tau_4 \frac{(126 - N)^2}{(126 - 82)^2} + \delta_{k,3}\, \theta_{43} \frac{(82 - Z)(Z - 50)}{(82 - 50)^2} \right] + \delta_{j,5}\delta_{k,4}\theta_{54} \frac{(184 - N)(N - 126)}{(184 - 126)^2} \times \frac{(126 - Z)(Z - 82)}{(126 - 82)^2}. \quad (10)$$

This mass law with the coefficients of the third column is the one used in most of the following calculations to represent shell effects. The additional terms have no known physical significance, and cannot be extrapolated across magic number closures. In particular, a coefficient θ_{53} to apply in the region $50 \leq Z < 82$, $126 \leq N < 184$ cannot be found. That these functions are not an adequate representation of deformations is demonstrated by the lack of fit of r-process calculations using this mass law to the deformation peak at $A = 164$.

iii) *Deformations and deformation energies.*—Nuclear deformations were calculated using the Nilsson (1955) model, with pairing correlations included (Bès and Szymański 1961; Wahlborn 1962). However, it was found that, if the model were applied strictly, all nuclei above $A = 40$ either had equilibrium deformations greater than $\epsilon = 0.5$, or would deform without limit. As this result is unreasonable, it was necessary to place a restriction on the model to insure stability, and to make magic nuclei spherical. This was accomplished by imposing a strict selection rule, such that for any number of particles between magic number N_j and magic number N_{j+1}, all levels which are below $N_j/2$ in the *spherical* nucleus must be occupied, even though at high deformation some such levels have a considerably higher energy than some unoccupied levels, and also no levels which are above $N_{j+1}/2$ in the spherical case are allowed to be filled, even though

TABLE 6

MASS LAW COEFFICIENTS IN MEV

Column Number	1	2	3	4	5	6	7
Mass Law Eq.	(8)	(9)	(10)	(9)	(11)	(11)	(11)
α	16.391	16.531	16.562	16.527	16.685	16.660	16.604
β	27.03	34.14	34.06	33.22	33.53	33.90	33.90
γ	21.052	21.383	21.467	21.33	21.992	21.845	21.568
η	31.2	65.7	65.8	62.0	62.4	64.3	64.6
δ	10.9	10.9	11.16	11.0	12.2	11.98	11.84
ζ_1		3.6	4.92	4.9	same as column 4	7.37	11.9
ζ_2		17.2	20.12	19.1		21.14	22.4
ζ_3		36.0	42.7	40.1		43.6	44.7
ζ_4		10.1	46.7	29.7		24.96	9.2
ζ_5		7.5	98.2	71.1		69.8	57.1
τ_4			-40.4				
θ_{43}			183.				
θ_{54}			513.				
Φ_1					12.0	same as column 5	6.9
Φ_2					6.4		2.9
Φ_3					-1.8		0.1
Φ_4					-9.9		-21.3
Φ_5					-6.2		-14.3
ν_1					-30.8	same as column 5	- 2.2
ν_2					-12.3		- 4.3
ν_3					15.		15.
ν_4					31.		28.
ν_5					220.		232.
σ (MeV)	2.971	1.652	0.850	0.953	1.149	1.107	1.000

at high deformation some of those levels have much lower energy. With these restrictions, the calculated deformations, as shown in Figure 7, agree reasonably with experiment (Mottelson and Nilsson 1959).

Attempts to use the deformation-energy calculated directly by the Nilsson model were not successful, but this was not surprising, as the model is not generally used to calculate energies. Therefore, the deformation energy was calculated by making known corrections of order ϵ^2 to terms in the standard mass law, and adding additional linear and quadratic terms in ϵ. The surface terms (γ and η in eq. [8]) were multiplied by the

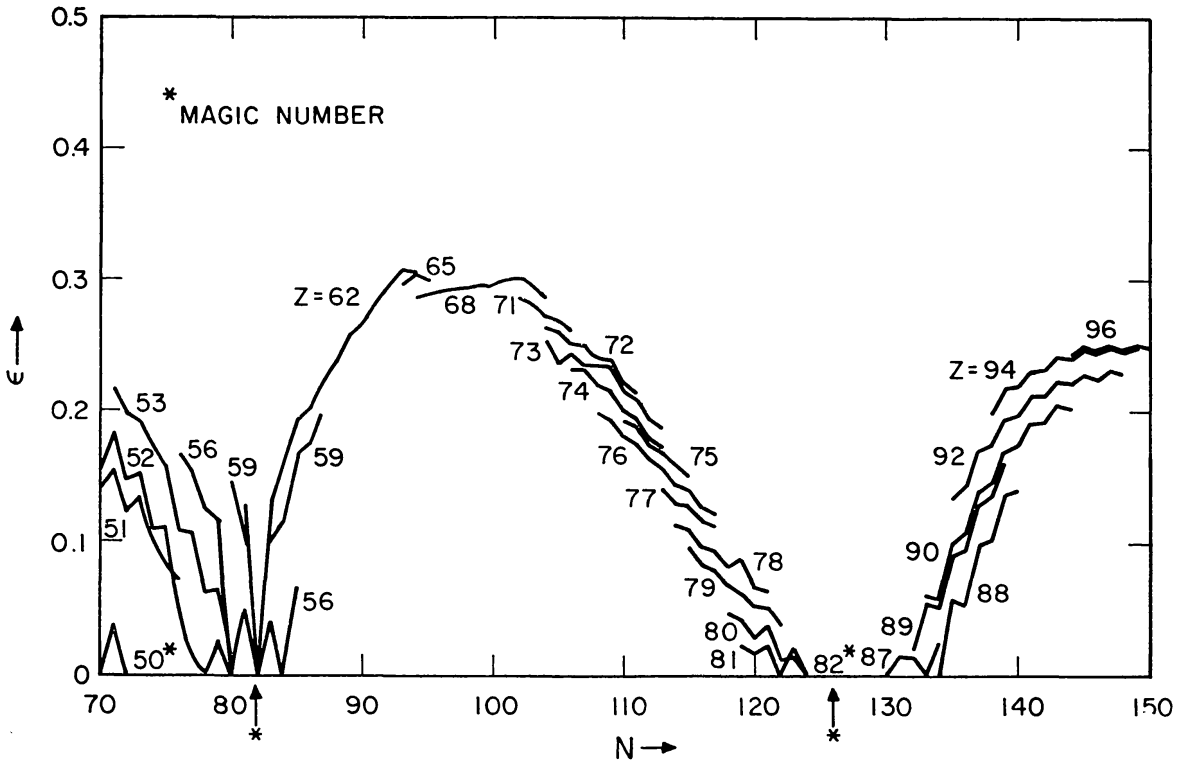

FIG. 7.—Equilibrium deformations for various Z. The Nilsson deformation parameter ϵ is plotted versus N for elements with Z between 50 and 96.

factor by which the surface area increases under deformation: $(1 + 2/45\ \epsilon^2 + 32/2835\ \epsilon^3)$. The Coulomb energy was multiplied by $(1 - 4/45\ \epsilon^2 - 2/81\ \epsilon^3)$. Then

$$B_D(Z, A) = B_s'(Z, A) + (\Phi_j + \Phi_k)\epsilon + (\nu_j + \nu_k)\epsilon^2 , \qquad (11)$$

where the coefficients Φ and ν vary from shell to shell, and the indices j and k are the same as in the shell-effects terms.

Results of adjustments of this modified mass law to the 825 empirical mass data for nuclear species with both N and Z greater than or equal to 20 are given in the fifth, sixth, and seventh columns of Table 6. In the fifth column the deformation coefficients were found while the shell-effects terms were held equal to the values found in the fourth column; then the deformation terms were held constant while the shell coefficients were recalculated (sixth col.). The changes in the coefficients ζ are not statistically significant. The effect of the correlation between ζ and Φ and ν is seen by the differences seen in the seventh column, the solution when all coefficients are found simultaneously. The coefficients of the sixth column are the ones used to represent deformations.

b) Thermal Equilibrium Calculations

Suppose a unit amount of element Z in equilibrium with a neutron density of n_n cm^{-3} at a temperature T_9 in units of 10^9 ° K; the ratio of the abundance of isotope $A+1$ to isotope A is given by (B^{2}FH 1957)

$$\log \frac{n(Z, A+1)}{n(Z, A)} = \log \frac{\omega(Z, A+1)}{\omega(Z, A)} + \log n_n - 34.07 - \tfrac{3}{2} \log T_9 + \frac{5.04}{T_9} Q_n(Z, A), \quad (12)$$

where $Q_n(Z, A)$ is the binding energy of the next neutron to nucleus (Z, A), given by

$$Q_n(Z, A) = B(Z, A+1) - B(Z, A) . \quad (13)$$

The factor $\omega(Z, A)$ is the sum over all states of the nucleus (Z, A) of the statistical weight of the state times the Boltzmann factor:

$$\omega(Z, A) = \sum_{i=0}^{\infty} (2J_i + 1) e^{-E_i/kT}, \quad (14)$$

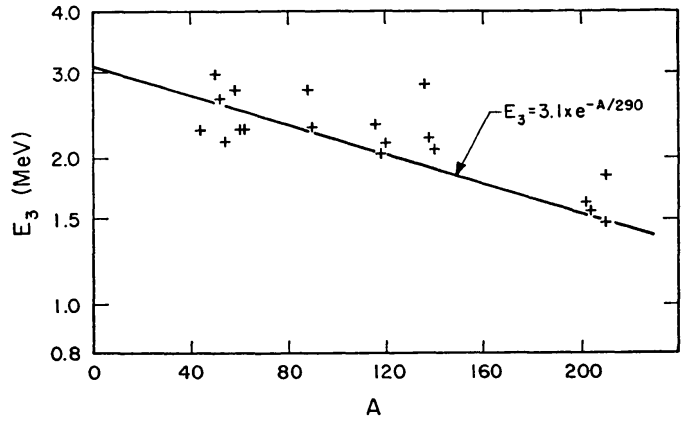

FIG. 8.—The energy of the third excited state of even Z, even N nuclei with either N or Z within 1 of a magic number is plotted versus A. The line is used as an approximation of this quantity.

where J_i is the spin and E_i the energy of state i. For these calculations, in which $kT \sim$ 100 keV, $\omega(Z, A)$ has been approximated as being proportional to the number of states in the nucleus within about $\frac{1}{4}$ MeV of the ground state. (A level at 230 keV would be about 10 per cent occupied.) Thus

$$\omega(Z, A) \propto 1 + \frac{0.25}{\Delta(Z, A)}, \quad (15)$$

where $\Delta(Z, A)$ is an approximate average level spacing (in MeV) for low-lying levels of nucleus (Z, A). Values of Δ were estimated by studying the observed level spacings reported in the Nuclear Data Sheets, the energy of the third excited state being taken as 3Δ. As the spacing is different for nuclei which are nearly magic or are deformed, plots were made versus A for the following categories of nuclei: M–M, meaning both N and Z within one of a magic number; M, if either N or Z is within one of a magic number; deformed, if A is in the range $150 \leq A \leq 190$ or $220 \leq A$; and spherical otherwise. Even Z, even N nuclei, odd A nuclei, and odd Z, odd N nuclei were considered separately. Figure 8 shows one plot, that for the even-even, M category. Eye fits of the form $E_3 = ae^{-A/b}$ were made to the plots. An average value of b was taken to be 290, and the a-value re-estimated. The results, expressed as the number of excited states below 1 MeV, are

given in Table 7. The spin degeneracy of each state, $(2J_i + 1)$, has been taken as constant when averaged over states. In the absence of any reasonable approximation for the effects of this term, it is thought that such effects would be within the other uncertainties of the calculations.

Then for given values of n_n and T_9 the ratios $n(Z, A + 1)/n(Z, A)$ can be found, and by normalizing to unit amount of element Z, the relative abundances $p(Z, A) = n(Z, A)/\Sigma_A n(Z, A)$ are determined. It was found that the distributions $p(Z, A)$ for any specific temperature were very sharp; i.e., only one or two values of A exist in any significant amounts. Then as Z varies in integer steps, every third or fourth value of A would be completely bypassed. This result is not observed in the abundances because the r-process has occurred across regions in which there is some variation in temperature, so that the distributions $p(Z, A)$ will be broadened to include more values of A. Therefore, the above calculations were performed at each of five distinct temperatures: T_9, $T_9 \pm 5$ per cent, and $T_9 \pm 10$ per cent. The $p(Z, A)$'s were then taken as a weighted average:

$$p(Z, A) = \tfrac{1}{16}\,[p(Z, A, 0.90\ T_9) + 4p(Z, A, 0.95T_9) + 6p(Z, A, T_9) + 4p(Z, A, 1.05\ T_9) + p(Z, A, 1.10\ T_9)]\ . \tag{16}$$

Although this temperature-spread smoothing helped greatly in the dropout problem, it was still found necessary to provide additional smoothing in the final results. The range of r-process environments that have contributed to solar-system material is apparently broader than represented in equation (16).

TABLE 7

DENSITY OF NUCLEAR STATES

($e^{-A/290}$ × Number of States within 1 MeV of Ground State)

	$M-M$	M	Spherical	Deformed
Even-even nuclei.....	0.22	0.97	1.36	2.73
Odd mass nuclei.....	0.60	1.67	5.0	8.6
Odd-odd nuclei.....	7.5	8.6	15	15

Figure 9 shows the distributions $p(Z, A)$ for the even N isotopes of two elements ($Z = 32$ and $Z = 79$) both with fixed temperature and with the temperature spread, for a neutron density of 10^{24} cm^{-3} and temperature $T_9 = 1.0$. Figure 10 illustrates the path of the r-process in the N–Z-plane for this density and temperature. It is found empirically that this same path is followed for $T_9 = 1.2$, $n_n = 10^{26}$ and also for $T_9 = 0.8$, $n_n = 10^{22}$. The empirical relation between values of T_9 and n_n which result in identical solutions is discussed in Section V*a* below.

The hypothesis of thermal equilibrium must be examined. Since the beta-decay rates will be shown to be of the order of 1/sec per nucleus, the condition which must be satisfied to obtain equilibrium is that the (n, γ) and (γ, n) rates must be fast compared to unity. Consider the (n, γ) rate. We can assume a typical neutron-capture cross-section to be 0.10 barn or 10^{-25} cm^2. Determining the neutron velocity v from $kT = \frac{1}{2}M_n v^2$, the (n, γ) rate for any nucleus (Z, A) is

$$\lambda_n(Z, A) = n_n \langle \sigma(Z, A)v \rangle \sim 4 \times 10^{-17} n_n T_9^{1/2}\ \text{sec}^{-1}\ \text{per nucleus.} \tag{17}$$

Thus the (n, γ) rates are sufficiently rapid for temperatures in the $T \sim 1$ range if $n_n \gtrsim 10^{18}$ cm^{-3}. For lower densities the s-process or some combination of the two would occur.

Consider then the inverse (γ, n) rate for nucleus (Z, A). At equilibrium

$$\lambda_\gamma(Z, A)n(Z, A) = \lambda_n(Z, A-1)n(Z, A-1)\,, \tag{18}$$

so

$$\lambda_\gamma(Z, A) = \lambda_n(Z, A-1)\frac{n(Z, A-1)}{n(Z, A)} \sim 4\times 10^{-17}\frac{n(Z, A-1)}{n(Z, A)}\, n_n T_9^{1/2}\ \text{sec}^{-1}\ \text{per nucleus}\,, \tag{19}$$

where $n(Z, A-1)/n(Z, A)$ would be the ratio of abundances if equilibrium occurred, as calculated by equations (12) and (16). It is found that for light isotopes, the (γ, n) rate is too slow by many orders of magnitude. This means that no (γ, n) reactions will occur to balance the (n, γ) reactions, and hence the light isotopes will be destroyed extremely rapidly. The lowest A which can exist in equilibrium for a given Z is that for which $\lambda_\gamma(Z, A') \gtrsim 1$ for all $A' > A$. In general this does not impose a restriction on the calculations, for it is found that the condition is satisfied for all isotopes (Z, A) which have

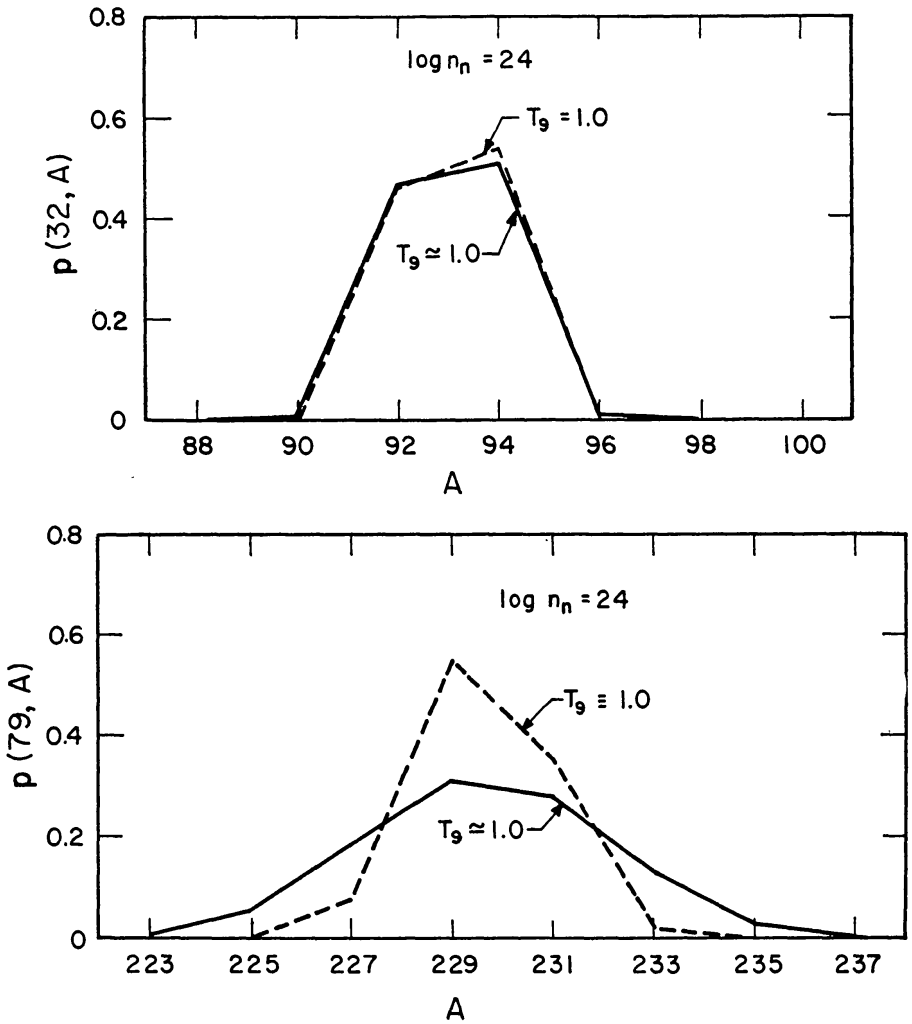

FIG. 9.—Relative isotopic abundances of Ge (*top*) and Au (*bottom*). Relative abundances of even N isotopes are plotted versus A both for fixed temperature and the temperature spread of equation (16). In the case of Ge ($Z = 32$) the spread of temperatures makes little difference, but for Au ($Z = 79$) the distribution is broadened.

any significant abundance at equilibrium. Table 8 lists the relevant rates in seconds for even isotopes of Ge and Au at two temperatures (see also Fig. 9). The odd isotopes have comparable λ_β and much greater λ_γ than their even neighbors. We conclude that the thermal equilibrium approximation is valid for temperatures above $T_9 = 1.0$ and log n_n above 22. For lower T_9 or log n_n, if thermal equilibrium is not valid, the path should be shifted one or two units higher in N, so that calculations assuming thermal equilibrium at a given temperature actually correspond to a slightly lower temperature.

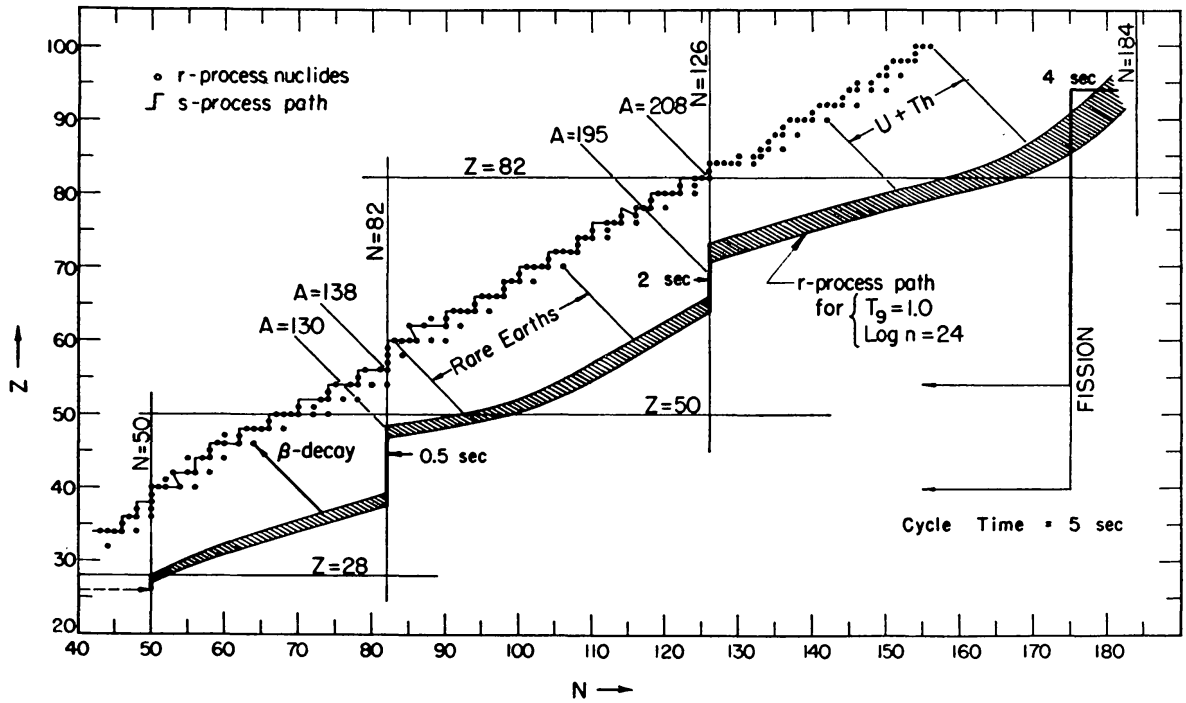

FIG. 10.—Neutron-capture paths. The *s*-process follows a path in the N–Z-plane which is near the line of beta-stability, and is represented by the single line. The *r*-process progenitor nuclei occupy a band in the neutron-rich area of the N–Z-plane, such as the shaded area here (calculated for $T_9 = 1.0$, log $n_n = 24$). Subsequently the progenitors beta-decay to the stable nuclei represented by circles; in many cases these end products of the *r*-process are also produced in the *s*-process. The observed abun dance peaks at $A = 130$ and $A = 138$ are attributed to the magic neutron number 82, and the peaks at $A = 195$ and $A = 208$ to $N = 126$. As neutrons are captured in the *r*-process, material starting at $Z = 26$ in the lower left-hand corner moves up the shaded band, reaching the $A \sim 130$ peak 0.5 sec and the $A \sim 195$ peak 2 sec after starting. After 4 sec material begins to reach $Z = 94$, where neutron-induced fission occurs; then a cyclic situation is established, and the number of nuclei is doubled by fission every 5 sec.

c) Probability of Beta-Decay

Having determined the isotopic distribution at a given Z, we must next determine the total probability for beta-decay to element $Z + 1$. First consider one isotope (Z, A) which decays to $(Z + 1, A)$. The assumption is made that every occupied state of the parent nucleus (Z, A) can decay to about every third state of the daughter nucleus $(Z + 1, A)$ with a value of log *ft* ranging from 5 at $Z = 20$ to 6.5 at $Z = 100$. Since the decay energy W_o to the ground state is typically about 15 MeV, and the excitation in the parent nucleus is only 100 keV, the decay probability from all occupied states is essentially the same, and hence the decay probability of nucleus (Z, A) is independent of its level density and of the temperature. It is therefore sufficient to consider all of the parent nuclei (Z, A) to be in the ground state.

States in the daughter nucleus with excitation between 0 and W_o are available for beta-decay; the probability of finding a suitable state in the range dE is $dE/3\Delta$, where Δ is the average level spacing of the *daughter* nucleus, taken from Table 7. The factor $\frac{1}{3}$ is

TABLE 8

RELATIVE ABUNDANCES AND DECAY RATES IN SEC^{-1}

Z	N	A	λ_β	$T_9 = 1.0$, $\log n_n = 24.$ p(Z,A)	λ_γ	1.4, 24. p(Z,A)	λ_γ	1.2, 22. p(Z,A)	λ_γ
32	52	84	1.61			0.0031	5.6×10^2	0.0042	0.96
	54	86	7.00			.2349	8.0×10^3	.3044	20.
	56	88	15.1			.6521	2.5×10^4	.6309	62.
	58	90	29.1	0.0102	54.	.1088	8.3×10^4	.0603	2.1×10^2
	60	92	51.6	.4679	4.6×10^2	0.0004	4.7×10^5	0.0001	2.0×10^3
	62	94	85.6	.5111	1.5×10^3				
	64	96	135.	0.0107	6.1×10^3				
79	130	209	0.507			0.0092	9.5×10^4	0.0174	4.6×10^2
	132	211	0.849			.0666	2.2×10^5	.0972	1.0×10^3
	134	213	1.36			.1977	2.7×10^5	.2432	1.2×10^3
	136	215	2.08			.3039	3.1×10^5	.3203	1.3×10^3
	138	217	3.08			.2614	4.0×10^5	.2270	1.6×10^3
	140	219	4.43			.1235	4.5×10^5	.0804	1.8×10^3
	142	221	6.22			.0275	5.6×10^5	.0110	2.6×10^3
	144	223	8.52	0.0052	1.1×10^4	0.0015	1.2×10^6	0.0002	8.0×10^3
	146	225	11.4	.0541	2.9×10^4				
	148	227	15.1	.1871	3.7×10^4				
	150	229	19.6	.3126	5.2×10^4				
	152	231	25.1	.2795	5.5×10^4				
	154	233	31.7	.1311	5.8×10^4				
	156	235	39.6	.0275	6.9×10^4				
	158	237	48.9	0.0014	1.4×10^5				

from the stated assumption that one-third of the states are fed by any single parent nucleus state. Now the customary approximation $f(Z, W) \approx \frac{1}{30}(W/m_oc^2)^5 \approx W^5$ (for f in sec^{-1} and W in MeV) is valid (Evans 1955) only for very low Z. For $Z = 80$ and $W = 15$ MeV this approximation gives a value of f which is too low by a factor of 10; that is, if the true value of log ft were 6, the approximation would give 5. But this error is similar to the observed variation of the ft value, so that by assuming log $ft = 5$ and $f(Z, W) = W^5$, a useful approximation for the mean life t is obtained. Then integrating over all the daughter states, taking W_o and Δ in MeV,

$$f = \int_0^{W_o} (W_o - E)^5 \frac{dE}{3\Delta} = \frac{W_o^6}{18\Delta} \text{ sec}^{-1}. \tag{20}$$

Taking log $ft = 5$, the probability of beta-decay of nucleus (Z, A) is

$$\lambda_\beta(Z, A) = \frac{10^{-5}}{18 \ln 2} \frac{W_o^6}{\Delta} \text{ sec}^{-1}. \tag{21}$$

The energy W_o is equal to the *nuclear* mass difference:

$$\begin{aligned} W_o &= [M(Z, A) - M(Z+1, A) + m_o]c^2 \\ &= B(Z+1, A) - B(Z, A) + (M_n - M_p)c^2 \\ &= B(Z+1, A) - B(Z, A) + 1.29 \text{ MeV}. \end{aligned} \tag{22}$$

Having found the decay probability λ_β for each isotope (see, e.g., Table 8), it is only necessary to take a weighted sum to find the total beta-decay probability, using the equilibrium abundance distributions found in Section IV*b*:

$$\lambda_Z = \sum_A p(Z, A) \lambda_\beta(Z, A) \text{ sec}^{-1}. \tag{23}$$

The mean life for material of a given Z is $t(Z) = 1/\lambda_Z$ sec. Although the $\lambda_\beta(Z, A)$ are independent of n_n and T_9, the quantities λ_Z and $t(Z)$ depend on n_n and T_9 through the abundances $p(Z, A)$. Figure 11 is a plot of the $t(Z)$ obtained for $T_9 = 1.0$ and log $n_n = 24$. These mean lives are quite different from those used by B^{2}FH (1957), because of differences in the path, in the assumptions concerning excitation in the daughter nuclei, and in the mass law. The calculations are subject to systematic errors, but should produce the main trends of beta-decay mean lives.

d) Isobaric Abundances

In general, the time rate of change of $n_Z(t)$, the amount of element Z at time t, is given by

$$\frac{d}{dt} n_Z(t) = +\lambda_{Z-1} n_{Z-1}(t) - \lambda_Z n_Z(t). \tag{24}$$

The set of coupled differential equations thus formed is solved subject to relevant boundary conditions. The first solution is for the initial condition $n_{26}(0) = N_o$, $n_{Z \neq 26}(0) = 0$; i.e., at time $t = 0$ there are N_o units of iron.

As more and more neutrons are added to the nuclei, fission will finally terminate the chain. However, in this solution no account is taken of fission; neutrons are added indefinitely until the material falls off the end of the computer. Hence this solution is valid only for short times, up to the time that recycling by fission commences.

A second form of solution is valid at times long compared to the sum of all beta-decay lives $t(Z)$. In this case fission interrupts the neutron-capture chain at a terminal value of

Z, and provides a continuous insertion of material at two values of Z representing the fission fragments. Thus a cyclic flow situation is established.

i) *Short-time solution.*—An analytic solution of the differential equation system was given some years ago by Bateman (1910). If

$$n_{26}(t) = N_o e^{-\lambda_{26} t}, \quad \frac{dn_Z(t)}{dt} = +\lambda_{Z-1} n_{Z-1}(t) - \lambda_Z n_Z(t); Z = 27, 28, \ldots, \tag{25}$$

then

$$n_Z(t) = N_o \sum_{i=26}^{Z} \left\{ \frac{\lambda_i}{\lambda_Z} \left[\prod_{\substack{j=26 \\ j \neq i}}^{Z} \frac{\lambda_j}{(\lambda_j - \lambda_i)} \right] e^{-\lambda_i t} \right\}. \tag{26}$$

Obviously this form of the solution is incorrect if any $\lambda_j = \lambda_i$ for $j \neq i$, but the possibility of this happening is remote, with all the λ_Z calculated to eight "significant"

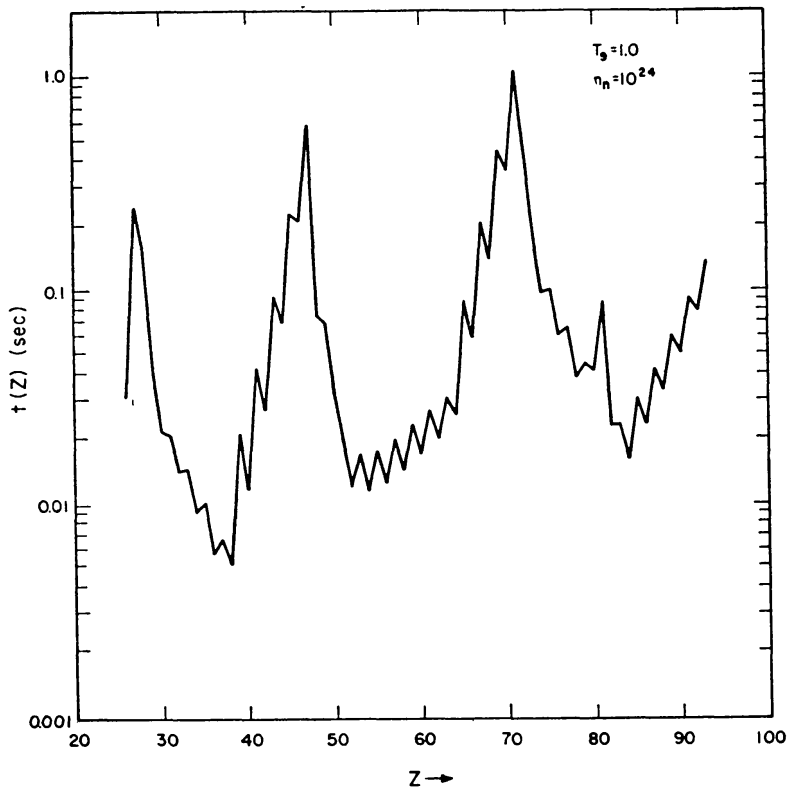

FIG. 11.—Beta-decay mean life. The mean life for beta-decay of the isotopes of each Z is plotted versus Z.

figures. Another difficulty in making numerical calculations with this expression is that for high Z at short times, it is necessary to calculate a very small number as a sum and difference of sixty or so very large numbers. However, any anomalies can easily be seen and rejected, and no other difficulties were encountered. In most cases, for any time t within the range of validity of the short-time solution, the sum over Z of the calculated abundances $n_Z(t)$ was within one part in 10^4 of the initial value N_o.

The number of atoms N_o was arbitrarily taken to be 50, in order to give results con-

veniently scaled for comparison with Figure 6. Then, knowing the number of atoms of each element existing at the time t when the process was halted, we can find the isobaric distribution by summing:

$$n_A = \sum_Z n_Z(t)\, p(Z, A), \tag{27}$$

where $p(Z, A)$ are the individual statistical distributions found in Section IV*b*.

Many n_A were factors of 10 lower than their neighbors, which is not the case in Figure 6. Hence it is apparent that some smoothing occurs. One source of smoothing is the occurrence of a range of environments within any one event; an arbitrary spread has already been included in the determination of the $p(Z, A)$ in equation (16). Either the assumed range in equation (16) must be extended, or other sources of smoothing must be considered. Two possibilities are the (n, γ) or (γ, n) reactions (whichever predominate) which may occur during cooling, and the superposition of events of differing conditions. Since the observed abundances indicate more smoothing, each n_A was averaged with its neighbors according to

$$n_A \rightarrow 0.15\, n_{A-1} + 0.70\, n_A + 0.15\, n_{A+1}\,. \tag{28}$$

Although such smoothing will lessen any even-odd effect, it will not eliminate it if it exists. No even-odd effect was apparent in the results.

Solutions for three different durations for $T_9 = 1.0$ and $n_n = 10^{24}$ are shown in Figure 12; for times greater than the final time plotted, 3.54 sec, the short-time solution would no longer be valid due to fission.

ii) *Long-time solution.*—The extension of the r-process to high values of A is limited by the occurrence of nuclear fission. If T is a representative time for a low Z atom to be converted into a high Z atom which fissions, then at times long compared to T the fission rate will control the flow of material in the r-process. However, the number of atoms will be increasing exponentially, since fission will double the number of atoms in the time interval T. Thus the time dependence can be expressed as

$$n_Z(t) = n_Z{}^o e^{\Lambda t}\,, \tag{29}$$

and the system of differential equations becomes an algebraic system:

$$\Lambda n_Z{}^o = \lambda_{Z-1} n^o{}_{Z-1} - \lambda_Z n_Z{}^o\,. \tag{30}$$

The cycle time is $(\ln 2)/\Lambda$.

The boundary conditions are expressed as follows. Suppose there is some Z_f such that all nuclei of element Z_f which beta-decay to $Z_f + 1$ immediately fission to form one atom each of elements Z_1 and Z_2. The value $Z_f + 1$ at which fission occurs is determined from the criterion $Z^2/A\,[1 - 2\,(I^2/A^2)]^{-1} \leq 40$ (Hoyle and Fowler 1960). It was found that for all temperatures T_9 between 1 and 3 and all neutron densities between 10^{18} and 10^{32}, $Z_f = 93$. It is not necessary to consider the distribution of the neutrons between the fission fragments, since the two nuclei will quickly come into thermal equilibrium with the neutron flux. We take $Z_1 = 0.43\,(Z_f + 1)$ and $Z_2 = 0.57\,(Z_f + 1)$. Then the boundary conditions are

$$\begin{aligned} &n_Z{}^o = 0,\ Z < Z_1 \quad \text{or} \quad Z > Z_f\,, \\ &(\Lambda + \lambda_{Z_1}) n_{Z_1}{}^o = \lambda_{Z_f} n_{Z_f}{}^o\,, \\ &(\Lambda + \lambda_{Z_2}) n_{Z_2}{}^o = \lambda_{Z_2-1} n^o{}_{Z_2-1} + \lambda_{Z_f} n_{Z_f}{}^o\,. \end{aligned} \tag{31}$$

Letting $\psi_Z = \lambda_Z n_Z^o$ and $\psi_f = \lambda_{Z_f} n_{Z_f}^o$, the system to be solved is

$$\psi_{Z_1} = \frac{\lambda_{Z_1}}{\lambda_{Z_1} + \Lambda} \psi_f, \qquad \psi_{Z_2} = \frac{\lambda_{Z_2}}{\lambda_{Z_2} + \Lambda} (\psi_{Z_2 - 1} + \psi_f),$$

$$\psi_Z = \frac{\lambda_Z}{\lambda_Z + \Lambda} \psi_{Z-1}, \qquad \text{for} \quad Z_1 < Z < Z_2 \quad \text{and} \quad Z_2 < Z \leq Z_f. \tag{32}$$

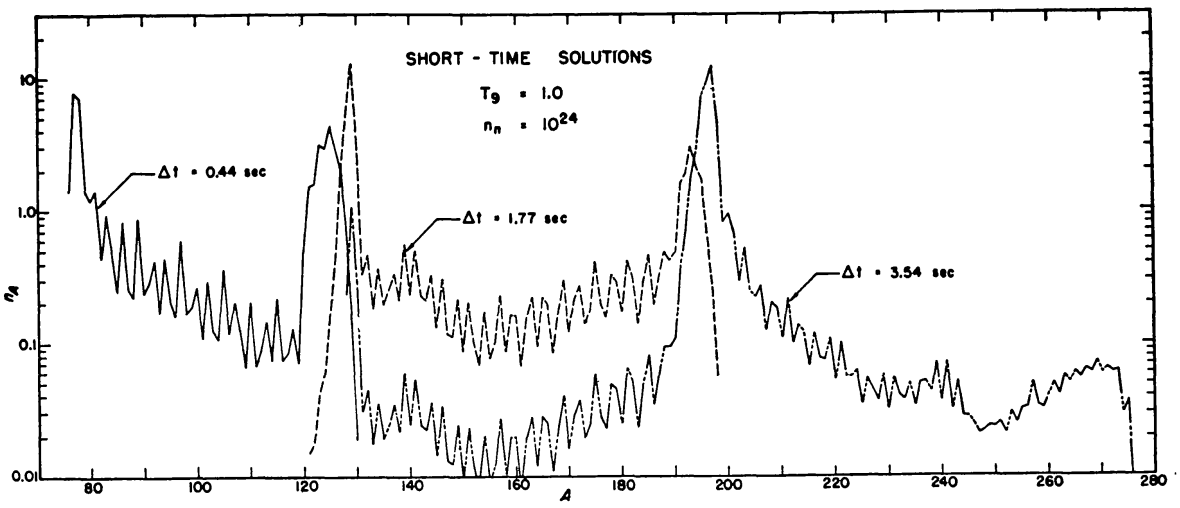

FIG. 12

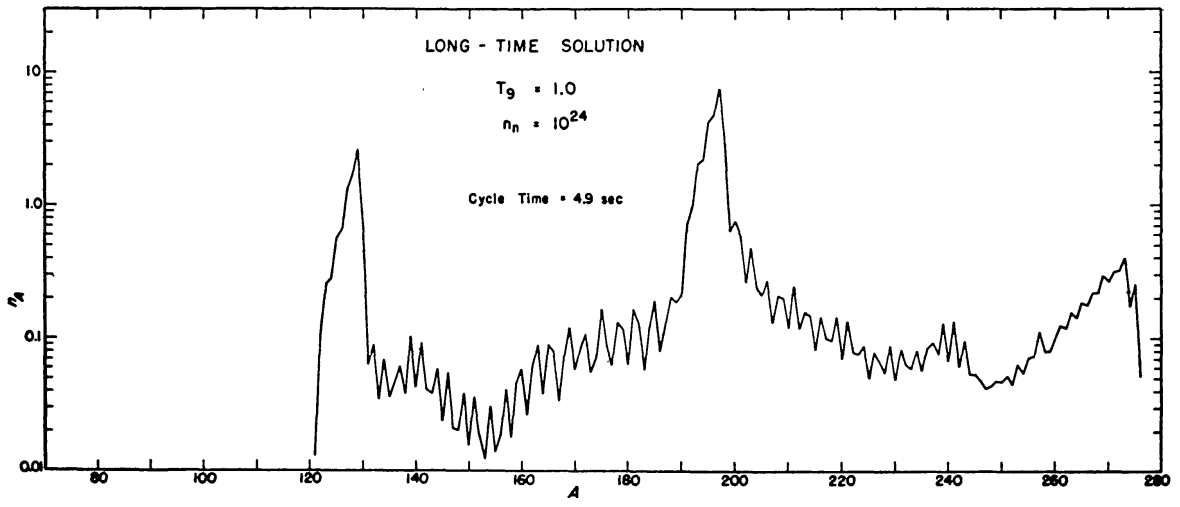

FIG. 13

FIG. 12.—Short-time solutions. Calculated r-process abundances are plotted for $T_9 = 1.0$, $\log n_n = 24$, and three durations.

FIG. 13.—Long-time solution. Calculated r-process abundances for long times for the same conditions as Fig. 12 are plotted. The relative abundances are constant with time, but the absolute scale doubles every 4.9 sec.

The unknown quantities to be found are the relative values ψ_Z/ψ_f, and the time constant Λ. The recursion relation can be applied successively to give an expression for each ψ_Z in terms of ψ_f:

$$\psi_Z = \prod_{i=Z_1}^{Z}\left(\frac{\lambda_i}{\lambda_i+\Lambda}\right)\psi_f, \qquad Z_1 \le Z < Z_2$$

$$\psi_Z = \left[\prod_{i=Z_1}^{Z_2-1}\left(\frac{\lambda_i}{\lambda_i+\Lambda}\right)+1\right]\prod_{i=Z_2}^{Z}\left(\frac{\lambda_i}{\lambda_i+\Lambda}\right)\psi_f, \qquad Z_2 \le Z \le Z_f. \tag{33}$$

This last expression must be an identity for the case $Z = Z_f$, and indicates what the value of Λ must be. Thus

$$\left[\prod_{i=Z_1}^{Z_2-1}\left(\frac{\lambda_i}{\lambda_i+\Lambda}\right)+1\right]\prod_{i=Z_2}^{Z_f}\left(\frac{\lambda_i}{\lambda_i+\Lambda}\right) = 1,$$

which can also be expressed

$$\prod_{i=Z_1}^{Z_f}\left(1+\frac{\Lambda}{\lambda_i}\right)-\prod_{i=Z_1}^{Z_2-1}\left(1+\frac{\Lambda}{\lambda_i}\right) = 1. \tag{34}$$

The expression on the left, when expanded in powers of Λ, is of order $Z_f - Z_1 + 1$. However, all coefficients are positive, and hence there is a unique positive root Λ. To find an upper limit on Λ, expand equation (34) in powers of Λ:

$$\Lambda\left(\sum_{i=Z_2}^{Z_f}\frac{1}{\lambda_i}\right)+\Lambda^2\left(\sum_{\substack{i=Z_1\\ j=i+1}}^{Z_f}\frac{1}{\lambda_i\lambda_j}-\sum_{\substack{i=Z_1\\ j=i+1}}^{Z_2-1}\frac{1}{\lambda_i\lambda_j}\right)+\ldots = 1. \tag{35}$$

Considering only the linear term, and noting that all terms are positive, the result is

$$\frac{1}{\Lambda} \ge \sum_{i=Z_2}^{Z_f}\frac{1}{\lambda_i}, \tag{36}$$

or that Λ is less than the harmonic mean of the beta-decay probabilities from Z_2 to Z_f. A value of Λ of any required accuracy can be quickly found numerically from equation (34). Then all the ψ_Z/ψ_f can be found from the recursion relation, and the $n_Z{}^o$ from $n_Z{}^o = \psi_Z/\lambda_Z$; the normalization used was $\Sigma n_Z{}^o = 50$ atoms.

The values n_A corresponding to the long-time solution are

$$n_A = \sum_Z n_Z{}^0 n(Z, A). \tag{37}$$

As in the case of the short-time solution, the results were smoothed by equation (28) before being plotted, as in Figure 13 for $\log n_n = 24$ and $T_9 = 1.0$. Comparison of this figure with Figure 12 shows that the short-time solution merges with the long-time solution essentially as soon as a few per cent of the atoms reach fission, and hence at times of the order of one characteristic time, $1/\Lambda$.

V. RESULTS OF r-PROCESS CALCULATIONS

Possible conditions under which the solar-system r-process material could have been produced will now be considered, followed by a brief discussion of possible sites for the synthesis.

a) Comparison of Calculations with Observations

The calculations of Section IV were carried out for a variety of conditions, with neutron densities between 10^{18} cm^{-3} and 10^{32} cm^{-3}, and temperatures between 0.6×10^9 ° K and 3.6×10^9 ° K. In each case short-time solutions were obtained for five appropriate durations, and the long-time solution was also calculated. It was found that whenever two solutions have the same cycle time then all other features of the two are essentially identical. Therefore solutions can be conveniently characterized by the cycle times, which are listed (in seconds) versus log n_n and T_9 in Table 9, and plotted in Figure 14. This table and figure are to be used to relate the features discussed below with the environments which could have produced them, and vice versa. It will be shown that no single environment and duration can produce the entire curve of Figure 6.

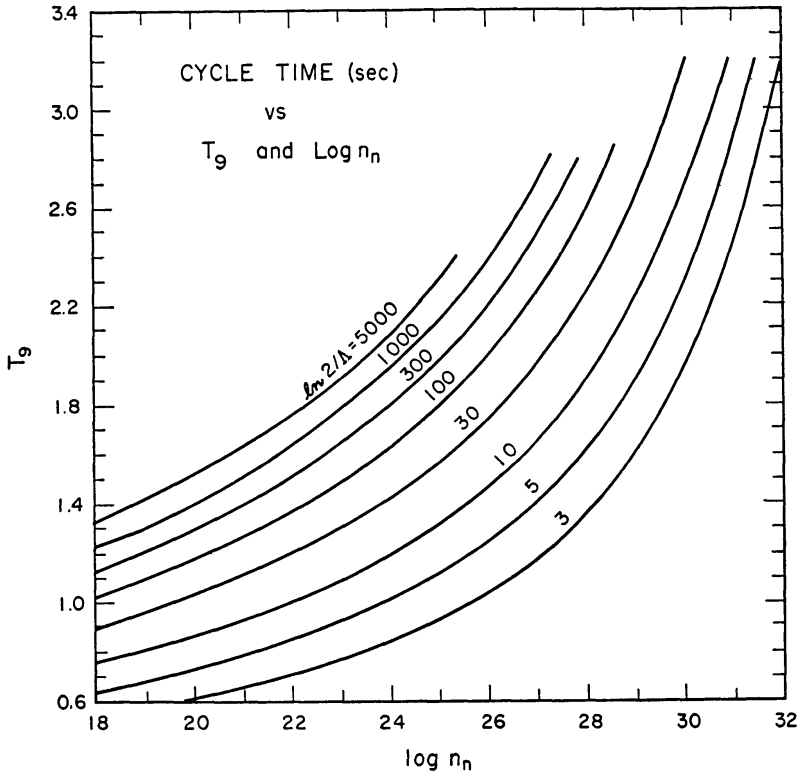

FIG. 14.—Cycle time. The cycle time ln 2/Λ (sec) is plotted versus T_9 and log n_n. Solutions for conditions with the same cycle time are essentially identical.

It should be pointed out that absolute times presented here are subject to considerable error due to the approximations and estimates made in Section IV*c* for the purpose of calculating beta-decay lifetimes. However, the errors should be largely systematic, either lengthening or shortening all times. Hence some such sequence of cycle times must exist.

i) $77 > A > 120$.—In this region it is possible to find solutions for which a very good fit is obtained to the location and height of the peak at $A = 80$, and to the general slope between $A = 95$ and $A = 120$. Another limitation on the acceptability of solutions in this region is that the height of the second major peak ($A = 130$) relative to the first must not be greater than the observed ratio, for no subsequent process acting on this material can enhance the first compared to the second. Even Marcus Aurelius appreciated this! This observation is significant, for it implies very short time scales. In Figure 15 the region labeled "First Peak" shows the locus of solutions for which the fit in this region is good; Figure 16 is a typical such solution (cycle time 370 sec, $\Delta t = 4$ sec).

TABLE 9

CYCLE TIME (SECONDS), ln 2/Λ

T_9	log n_n							
	18	20	22	24	26	28	30	32
0.6	4.21	2.86	.....	.....	.....	.....	.....	.....
0.8	13.4	7.12	4.28	2.65	.....	.....	.....	.....
1.0	83.3	24.2	10.1	4.90	2.70	.....	.....	.....
1.2	697	128	31.0	10.5	4.50	2.33	.....	.....
1.4	7.7×10^4	1.0×10^3	135	26.8	8.04	3.17	1.74	.....
1.6	.....	9.2×10^4	804	96.4	16.7	4.88	2.09	.....
1.8	.....	4×10^9	1.8×10^4	307	38.5	7.76	2.56	1.38
2.0	.....	.....	2×10^7	2.1×10^3	110	13.4	3.27	1.47
2.2	.....	.....	.....	7.8×10^4	295	24.7	4.47	1.59
2.4	.....	.....	.....	.....	1.3×10^3	50.9	6.20	1.76
2.6	.....	.....	.....	.....	.....	113	8.89	1.98
2.8	.....	.....	.....	.....	.....	243	13.3	2.25
3.0	.....	.....	.....	.....	.....	.....	20.7	2.59
3.2	.....	.....	.....	.....	.....	.....	32.8	3.05
3.4	.....	.....	.....	.....	.....	.....	.....	3.66
3.6	.....	.....	.....	.....	.....	.....	.....	4.48

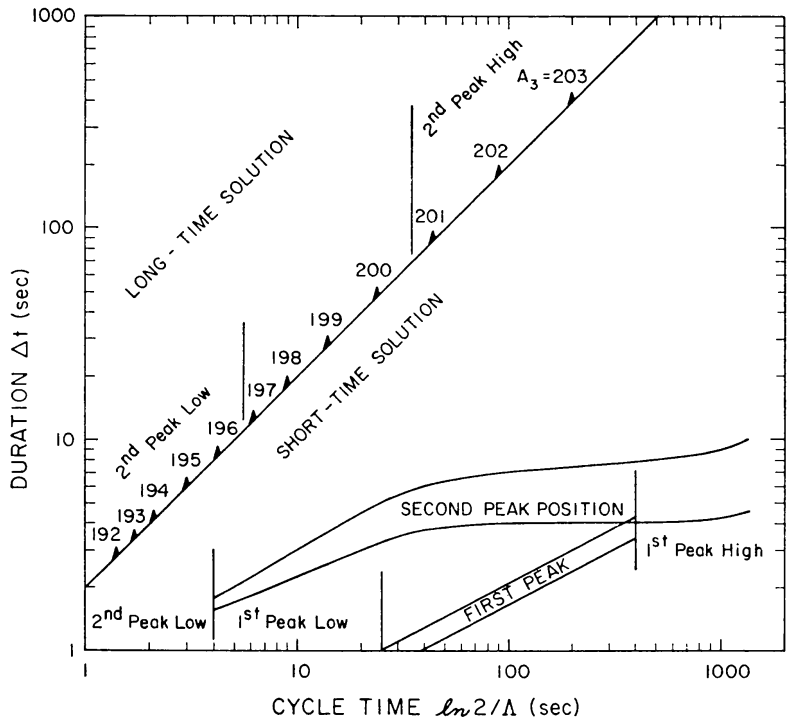

FIG. 15.—Analysis of r-process solutions. Various features of the solutions with given cycle times are indicated as functions of duration. (Conditions of temperature and neutron density can be related to cycle time by Fig. 14.) The region marked "First Peak" is the locus of solutions which fit the observed r-process abundances for $77 < A < 120$, and also have close to the observed abundance in the $A \sim 130$ peak. The region marked "Second Peak Position" indicates those solutions for which the $A \sim 130$ peak is properly located in the short-time solution; note the small overlap for which peak 1 and peak 2 are both correctly given. The long-time solution is taken to hold for durations longer than twice the cycle time. The calculated position A_3 of the third peak in the long-time solution is indicated as a function of cycle time along the diagonal line; the observed value of $A = 195$ implies a short cycle time.

Solutions with cycle times less than 25 sec produced the first peak at values of atomic weight more than one unit too low; those for cycle times greater than about 400 sec resulted in values of A too high by more than one. For durations shorter than those indicated by the first peak region in Figure 15, the slope between $A = 95$ and $A = 120$ was too steep, and for longer durations the second peak became too tall compared to the first. Since the first peak contains the bulk of the r-process material, it follows that the majority of the material was exposed to the neutron flux for only 1–5 sec; otherwise the first peak would have been destroyed.

Under none of the conditions considered did the r-process calculations produce a peak near $A = 84$, nor does it seem likely that any physically reasonable mass law will lead to such a structure. We therefore tentatively ascribe the krypton peak to the s-process (see Sec. III*d*[i], and Cameron 1959) until such time as experimental measurements of the krypton neutron-capture cross-sections become available.

ii) *Second peak*, A $\sim$ 130.—As seen in Figure 12, the second major peak begins to form quickly on the low A side, and moves about 4 or 5 units higher in A with time. It was found that for all cycle times between 4 sec and 10^5 sec there was some duration for which the location of the second peak was correct. These are indicated by the region labeled "Second Peak Position" in Figure 15. Thus the $A = 130$ peak imposes only slight restrictions on temperature and density, unless it is considered in relation to the other peaks.

If the second peak was produced simultaneously with the first, the choices are limited to cycle times of the order of 350–400 sec and durations of the order of 4 sec. Figure 16 is such a solution.

If, on the other hand, only a fraction of the second peak was produced in the same environment that gave the first peak, the balance may have been produced by cycling solutions in the type of event which produced the higher A material. In that case, in the cycling solution the height of the second peak relative to the third must be less than the observed value, which is of the order 3 (see Fig. 6). The position of the second peak is given correctly in the long-time solution for cycle times between 5.5 sec and 35 sec (see Figs. 13, 15). In all of these cases, however, the height of the second peak was only $\frac{1}{3}$–$\frac{2}{3}$ the height of the third peak, so only 10–20 per cent of the second peak would have been formed in this way; the majority of the material in the second peak would have to be produced in short-time rather than long-time events. However, due to the large uncertainty in the calculation of the third peak (see Sec. V*a*[iv]) this conclusion cannot be regarded as firm.

iii) $145 < A < 180$.—The broad peak at $A = 164$ in Figure 6 is thought to be due to deformation energy in the progenitor nuclei. Comparison with Figures 12 and 13 shows that the mass law of equation (10) does not reproduce this feature at all.

The only mass law tested which is capable of reproducing this peak is one containing deformation terms based on the Nilsson model (see Sec. IV*a*[iii], and the sixth column of Table 6). Figure 17 is a plot of the long-time solution using this mass law, for $T_9 = 1.2$ and $\log n_n = 24$. The general trend of the broad peak due to deformations is seen in the range $145 < A < 180$, but the fit in other regions is not particularly good, and local irregularities are even greater than for the mass law without deformations. We include this figure only to show that in the region where deformations are best understood, inclusion of semi-theoretical deformation terms is necessary to produce the observed hump in the abundance-curve.

To facilitate comparison with the experimentally well-known rare-earth abundances, the isotopic abundances of Figure 17 were summed to give elemental abundances, which were then normalized to the sum from $Z = 59$ to $Z = 71$ from Table 5, and entered in Table 10. Also shown in Table 10 are similarly normalized elemental abundances from the paper of Becker and Fowler (1959), who are the first authors to account quantitatively for the deformation hump.

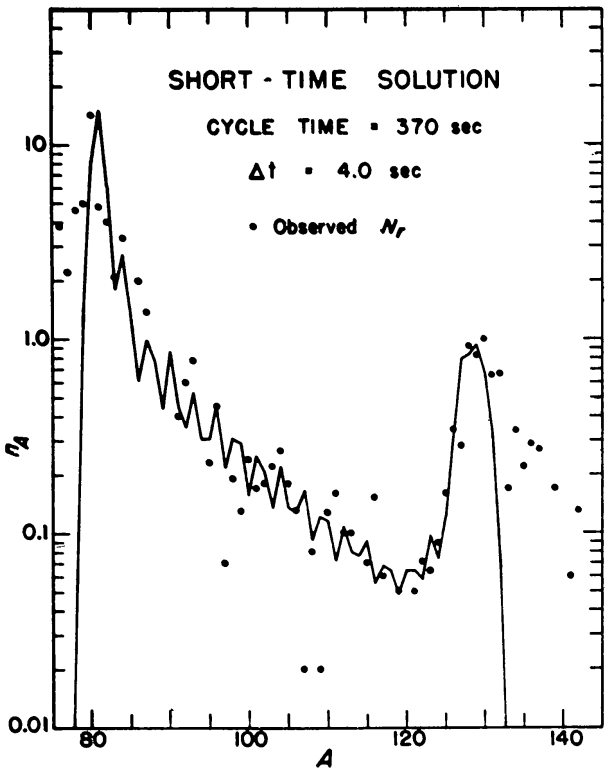

FIG. 16

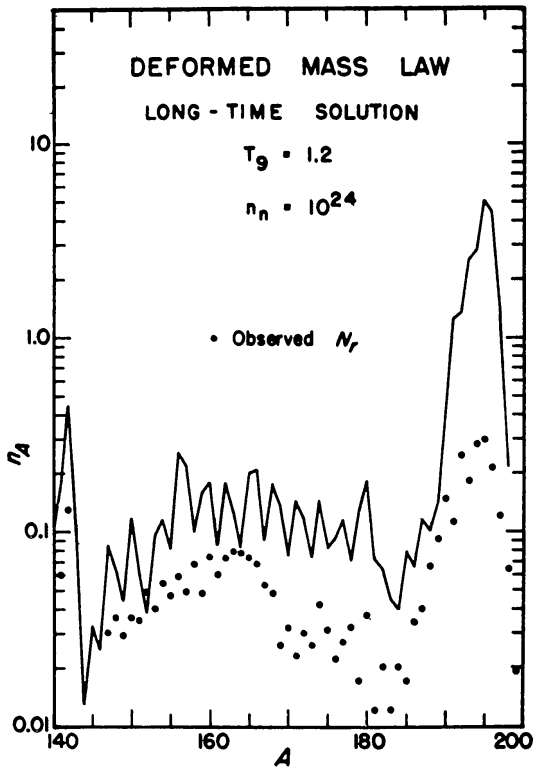

FIG. 17

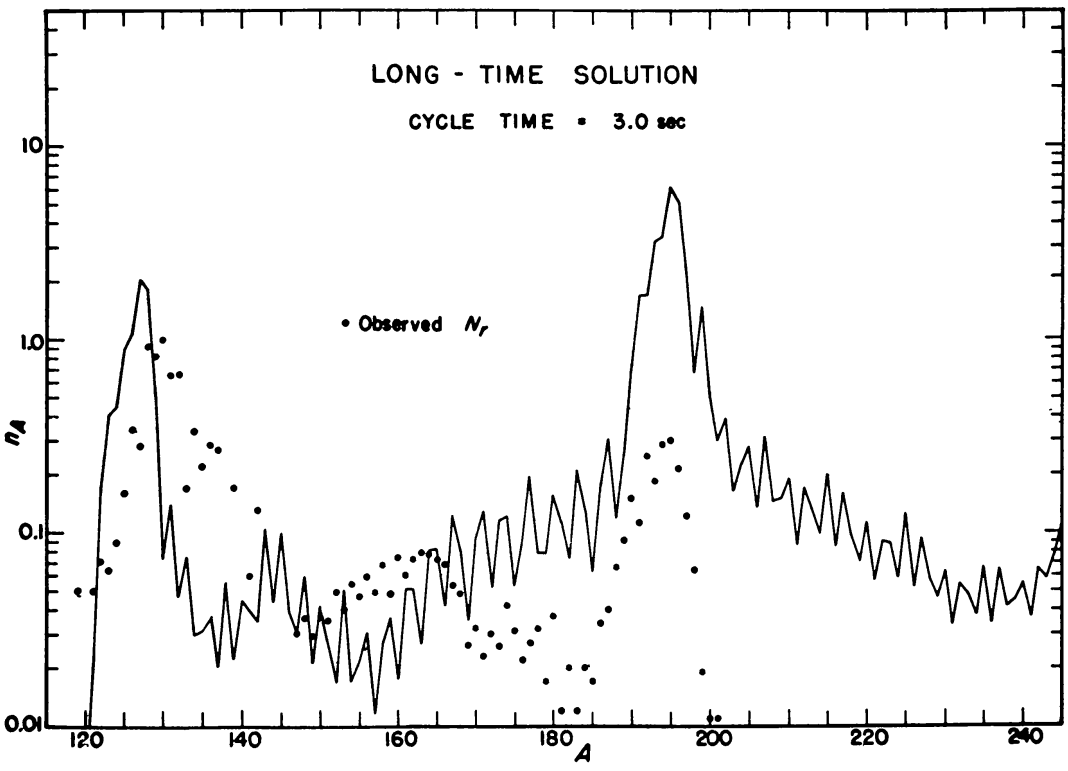

FIG. 18

FIG. 16.—Calculated r-process abundances. Reasonable agreement with observed solar-system r-process abundances in the range $78 < A < 130$ is obtained with cycle time 370 sec, duration 4.0 sec.

FIG. 17.—Calculated r-process abundances. The shape of the broad abundance peak in the rare earths is best fit by calculations using a mass law containing deformation terms.

FIG. 18.—Calculated r-process abundances. The location of the third major abundance peak is correctly given at $A = 195$ by a long-time solution with cycle time 3.0 sec. In this solution, the number of nuclei of each species doubles every 3.0 sec.

iv) *Third peak*, A $\sim$ 195.—For A greater than about 190, the calculations enter the region in which the mass-law extrapolation is most difficult. The r-process path (Fig. 10) then enters the area $N > 126$, $Z < 82$, in which there are virtually no known masses to determine local shell or deformation terms. The extrapolation of the mass surface must cross magic numbers in both N and Z. Very short cycle times (i.e., either high neutron densities or low temperatures) are required to get good agreement with the experimental position of the $A = 195$ peak using the mass law of equation (10). The location and height of the peak are very strong functions of the mass law used, and addition of arbitrary terms often leads to the complete disappearance of the peak. We are reluctant to vary the mass law to fit this peak, without other justification.

It can be firmly stated that it is impossible in the r-process as described here to have any material reaching the third peak while any remains in the first peak. Thus we must say that solar r-process material was produced in two distinct types of events: one type lasting about 4 sec to produce the first peak and most of the second, and another type

TABLE 10

RARE EARTH r-PROCESS ABUNDANCES

Element	Z	Observed	Becker and Fowler	This Work
Pr.....	59	0.06	0.020	0.069
Nd.....	60	.2	.251	.144
Pm.....	61	0	0	0
Sm.....	62	.163	.217	.115
Eu.....	63	.075	.097	.064
Gd.....	64	.30	.247	.338
Tb.....	65	.408	.064	.064
Dy.....	66	.29	.194	.190
Ho.....	67	.073	.064	.082
Er.....	68	.20	.202	.223
Tm.....	69	.026	.040	.054
Yb.....	70	.14	.187	.231
Lu.....	71	0.031	0.024	0.033

lasting for long enough times that cycling occurs. The location of the third peak as a function of cycle time is indicated along the line in Figure 15 which delimits the region in which the long-time solution is to be used. It is seen that solutions with cycle times of the order of 3 sec give the peak closest to the correct position. Figure 18 (cycle time = 3.0 sec) can be considered typical (see also Fig. 13, cycle time = 4.9 sec). Although the second peak is not correctly located in this solution, the amount of material in it is sufficiently small compared to the $A = 195$ peak that it would be hidden in a properly normalized superposition of this solution with one similar to Figure 16.

v) *Trans-lead region*, A > 210.—In the trans-lead region we have no direct experimental measurements on what the isotopic abundances would have been at the time nucleosynthesis occurred. It is of interest, however, to see what these r-process calculations predict as abundances of the parents of the radioactive series. The solution shown in Figure 18 cannot be used for this purpose because the r-process path (cf. Fig. 10) in that case comes too close to the limit of the mass law at $N = 184$, so that abundances above $A = 245$ cannot be calculated. Therefore, the solution of Figure 13 was used, with additional smoothing. Normalization to the scale Si = 10^6 was effected by summing the calculated abundances of the rare earths in the same figure and comparing to the similar sum from Table 4. Then the r-process yields for the progenitors of each radioactive series were entered in Table 11, and summed. The $(4n + 1)$ and $(4n + 3)$ series were reduced by 10 per cent and the $4n$ and $(4n + 2)$ series were increased by 10 per cent for

the even-odd effect, as determined by comparing sums of even and odd isotopes in the rare-earth region. The results are similar to those obtained previously (Fowler and Hoyle 1960); these calculations give $Th^{232}/U^{238} = 1.7$ and $U^{235}/U^{238} = 1.5$. However, the mass-law uncertainties prohibit a confident calculation of the level of these abundances.

A complementary calculation of the trans-uranic abundances involves their relationship to galactic chronology and the synthesis of lead. This method has been developed by Clayton (1963, 1964), but his numerical results must be tempered by present uncertainties in the approximate neutron capture cross-sections of the lead isotopes (Macklin and Gibbons 1964). Further work on this complicated problem is under way.

b) Astrophysical Site of the r*-Process*

The r-process requires the capture of a large number of neutrons per seed nucleus. If iron-group elements provide the seed nuclei then ~25 neutrons are required to form the first r-process peak at $A = 80$, ~75 neutrons are required for the peak at $A = 130$, ~140 neutrons are required for the peak at $A = 195$, and more than 220 neutrons are required if cycling is to be established after fission occurs. Thus the process can only occur where the ratio of free neutrons to seed nuclei is initially large.

TABLE 11

CALCULATED r-PROCESS ABUNDANCES FOR PARENTS OF THE RADIOACTIVE SERIES (Si = 10^6)

$Th^{232}(4n)$		$Np^{237}(4n+1)$		$U^{238}(4n+2)$		$U^{235}(4n+3)$	
A	Yield	A	Yield	A	Yield	A	Yield
232.....	0.049	.....	.....	.....	.....	235.....	0.054
236.....	.056	237.....	0.059	238.....	0.061	239.....	.065
240.....	.066	241.....	.065	242.....	.059	243.....	.051
244.....	.043	245.....	.038	246.....	.036	247.....	.032
248(0.89)..	.029	249.....	.033	250(0.10)..	0.004	251.....	.036
252(0.86)..	0.033	253.....	0.040	.....	.....	255.....	0.047
Total...	0.276	Total..	0.235	Total...	0.160	Total..	0.285
	×1.10		×0.90		×1.10		×0.90
	=0.30		=0.21		=0.18		=0.26

For this reason, Hoyle and Fowler (1960) suggested that the r-process must occur in material which is explosively expanding subsequent to the iron to helium-neutron phase change at the end of stable nuclear evolution. Upon rapid enough expansion, the reconversion of the helium back into heavier nuclei is limited by the rate of the $3\alpha \rightarrow C^{12}$ reaction. Subsequent alpha-particle and neutron captures rapidly convert the C^{12} into iron-group nuclei which then serve as seeds for the r-process. However, the low rate of C^{12} production guarantees that the seed nuclei are rare compared to the neutrons and alpha-particles which make up the bulk of the material in the ratio $n/\alpha \sim \frac{4}{13}$ from $Fe^{56} \rightarrow 13\alpha + 4n$. It is well known that He^4 does not capture neutrons, and it is thus inert insofar as the r-process is concerned.

Recent experimental measurements make it possible to improve upon the reaction rate estimate for $3\alpha \rightarrow C^{12}$ used by Hoyle and Fowler (1960). In the temperature range $1 < T_9 < 10$ the reaction proceeds through resonances in C^{12} at 7.65 MeV and 9.64 MeV for which the partial mean lifetimes in sec are

$$\log \tau_{3\alpha} = 9.25 - 2 \log \rho x_\alpha + 3 \log T_9 + 1.875/T_9, \text{ via } C^{12*}(7.65 \text{ MeV}) \quad (38)$$

and

$$\log \tau_{3\alpha} = 7.77 - 2 \log \rho x_\alpha + 3 \log T_9 + 11.91/T_9, \text{ via } C^{12*}(9.64 \text{ MeV}) . \quad (39)$$

When these are properly compounded it is found that a very good approximation for the mean lifetime in seconds over the entire temperature range of interest is

$$\log \tau_{3\alpha} = 11.13 - 2 \log \rho x_\alpha + 0.70 \log T_9 . \quad (1 < T_9 < 10) \tag{40}$$

Now consider this lifetime in connection with the conditions which give the fit to the peaks at $A = 80$ and 130 in Figure 16, namely $T_9 = 2.43$, $\log n_n = 26.7$, and $\Delta t = 4$ sec duration. For the formation of these two peaks in their observed proportions, an average of about 35 neutrons per seed nucleus are required so from the argument of Hoyle and Fowler (1960) $\tau_{3\alpha} \sim 35\ \Delta t \sim 140$ sec. With $x_\alpha \sim 52/56$ and $x_n \sim 4/56$ from $Fe^{56} \rightarrow 13\alpha + 4n$ and with $T_9 = 2.43$, equation (40) results in $\log \rho = 4.6$ and $\log n_n = 27.3$ initially. During the assumed 4-sec duration the density will change by a factor $1/e$, but the neutron mass fraction will drop from $\frac{4}{56}$ to essentially zero as the neutrons are consumed. There will be too few neutrons remaining per heavy nucleus to alter appreciably the abundance distribution as established. Also, it is quite possible that the path in the T_9, n_n plane followed during cooling would be parallel to one of the Λ = constant curves of Figure 14, in which case the solution would not change during cooling. However, it is the depletion of the neutrons which primarily leads to the freezing in of the abundances at relatively high temperature. The effective value for n_n during the r-process will be $\sim 1/e$ times the initial value or $\log n_n = 26.9$, in excellent agreement with the value 26.7 required for best fit at this temperature.

Hoyle and Fowler (1960) originally suggested that the site for the r-process was Type I supernovae which were taken to represent the explosive outburst of relatively low-mass stars in the range 1.2–1.5 $M_\odot$. However, the density-temperature relation for stars in this mass range did not yield the density and temperature required for the r-process as discussed above. Subsequently, Hoyle and Fowler (1963) suggested that proper conditions were more nearly met in massive stars, $M > 10^4\ M_\odot$, associated with extended and quasi-stellar radio objects. This suggestion is borne out by our present results as can be seen from the analysis now to be presented.

Free explosion is the reverse in time of free fall, and the time scale is closely comparable. Fowler and Hoyle (1964) give

$$\Delta t = dt/d \ln \rho = (24\pi G\rho)^{-1/2} = 446/\rho^{1/2} \text{ sec} . \tag{41}$$

In terms of the neutron density

$$n_n = \tfrac{4}{56}\rho \times 6 \times 10^{23} \sim 4.3 \times 10^{22}\ \rho , \tag{42}$$

equation (41) becomes

$$\Delta t \sim 10^{14}/n_n^{1/2} . \tag{43}$$

Thus for $\Delta t \sim 4$ sec (as required for simultaneous production of the first two peaks), $n_n = 5 \times 10^{26}$ or $\log n_n = 26.7$. From Figure 15 it is seen that a solution with cycle time ~350–400 sec is required; from Figure 14 a temperature $T_9 = 2.43$ is then found. (The solution for this temperature and neutron density is shown in Fig. 16.) The density corresponding to $\Delta t = 4$ sec is $\rho \sim 10^4$ gm cm^{-3}, and this value along with the temperature $T_9 = 2.43$ can be employed to fix the mass of the stars in which the r-process occurs.

Fowler and Hoyle (1964) give equations which reduce to

$$\rho \sim 2 \times 10^5 \left(\frac{M_\odot}{M}\right)^{1/2} T_9^3 \tag{44}$$

near $T_9 = 2.5$. This expression can be used as a fair approximation during the terminal stages of the free explosion of a star with $M > 10^3 M_\odot$. Solving for the stellar mass yields

$$M/M_\odot = 4 \times 10^{10} T_9^6/\rho^2 \quad (45)$$

and the conditions $T_9 = 2.43$, $\rho = 10^4$ then give $M/M_\odot = 10^5$. Considering the range of temperature and density conditions which could give satisfactory solutions,

$$M/M_\odot \sim 10^{5\pm1} \text{ (for } r\text{-process)} . \quad (46)$$

This result is in substantial agreement with the conclusions of Hoyle and Fowler (1963), to which the reader is referred for the detailed consequences of assigning the r-process to massive stars which evolve rapidly and are thus capable of producing r-process elements early in the history of the Galaxy as well as subsequently. The uncertainty indicated in equation (46) is an estimate based on the range of conditions which were found in Section V*a* to be suitable for production of r-process material in good agreement with the observed abundances of the r-nuclei. It is of interest to note that stars with masses in the range given by equation (46) are just those which Iben (1963) and Fowler (1964) suggest may well be disintegrated by explosive nuclear burning after the onset of general relativistic instability.

If the third r-process peak was synthesized in the same object, the relation $\rho \sim T_9^3$ from equation (44) can be compared with Figure 14 to find the conditions corresponding to a solution with cycle time 3 sec; the results are $T_9 = 1.0$, $\log n_n = 25.5$ as shown in Figure 18.

It becomes increasingly important to have some independent evidence for locating the r-process site, whether massive objects, conventional supernovae, or both.

VI. SUMMARY

We have analyzed the solar-system abundances of the heavy elements in terms of the s- and r-processes of nucleosynthesis. Observed abundances and cross-sections of nuclei assigned to the s-process are consistent with s-process theory, and indicate that the number of iron nuclei exposed to a given integrated neutron flux is a rapidly decreasing function of that flux; approximately $\rho(\tau) = 10000 \exp(-\tau/0.17)$, as shown in Figure 1. This distribution of exposures must be accounted for by the frequencies and efficiencies of the astrophysical events leading to the s-process, and the extent of readmixture into later generation s-process events. Knowledge of the s-process exposure distribution and environment can be improved by measurement of the neutron-capture cross-sections of the isotopes of Kr. If, as we have tentatively assumed, these unknown cross-sections are consistent with the synthesis of Kr^{84} and Kr^{86} in the s-process, the environment must have a temperature near 2×10^8 ° K, consistent with helium-burning neutron sources.

Table 4 and Figure 6 show the subtraction of s-process abundances and the residual empirical r-process abundances. The assumption that the peaks near $A = 80$, 130, and 195 are due to nuclei with $N = 50$, 82, and 126 lying along a rapid neutron-capture path demands a path such as shown by the shaded area in Figure 10, corresponding to an environment of high temperature ($\sim 10^9$ ° K) and high neutron densities ($\sim 10^{20} - 10^{28}$ cm^{-3}) lasting for short times ($\sim$ sec). All three peaks cannot have been produced under the same set of circumstances; an analysis of environments leading to specific features of the r-process abundance distribution is shown schematically in Figure 15. The existence of the $A = 80$ peak demands a very short-lived (~ 4 sec) r-process environment. This short time scale, if related to a free-fall time, implies a density consistent with conditions in an object with mass in the range 10^4–$10^6 M_\odot$. The general features of the r-process abundance-curve seem to be well understood in terms of nuclear physics, but the uncertainty of the form of the semi-empirical atomic mass law when extrapolated to very

neutron-rich nuclei introduces a fundamental impediment to the detailed calculations of abundances.

The semi-empirical division of the solar-system abundances into their *s*- and *r*-components has been made with greater accuracy and confidence than was possible in the past, and has been presented in tabular form (Table 5) as an aid to astronomical investigators of heavy-element nucleosynthesis.

Thus ends the "Handbuch der *sr*-Prozesse."

We wish to thank the many workers in the fields of elemental abundances and neutron-capture cross-sections who have made useful suggestions. In particular we appreciate the interest of R. A. Schmitt, who has called many current experimental abundance measurements to our attention, and we wish to thank J. H. Gibbons and R. L. Macklin for providing us with their cross-section data prior to publication.

REFERENCES

Bahcall, J. N. 1962, private communication.
Bateman, H. 1910, *Proc. Cambridge Phil. Soc.*, **15**, 423.
Becker, R. A., and Fowler, W. A. 1959, *Phys. Rev.*, **115**, 1410.
Bès, D. R., and Szymański, Z. 1961, *Nuclear Phys.*, **28**, 42.
Bethe, H. A., and Bacher, R. F. 1935, *Rev. Mod. Phys.*, **8**, 367.
Burbidge, E. M., and Burbidge, G. R. 1957, *Ap. J.*, **126**, 357.
Burbidge, E. M., Burbidge, G. R., Fowler, W. A., and Hoyle, F. 1957, *Rev. Mod. Phys.*, **29**, 547; referred to hereafter as B^{2}FH (1957).
Cameron, A. G. W. 1959, *Ap. J.*, **130**, 452.
Clayton, D. D. 1963, *J. Geophys. Res.*, **68**, 3715.
———. 1964, *Ap. J.*, **139**, 637.
Clayton, D. D., Fowler, W. A., Hull, T. E., and Zimmerman, B. A. 1961, *Ann. Phys.*, **12**, 331.
Evans, R. D. 1955, *The Atomic Nucleus* (New York: McGraw-Hill Book Co.), p. 559.
Fowler, W. A. 1964, *Rev. Mod. Phys.*, **36**, 545.
Fowler, W. A., and Hoyle, F. 1960, *Ann. Phys.*, **10**, 280.
———. 1964, *Ap. J. Suppl.*, **9**, No. 91, 1.
Goldberg, L. 1964, paper presented November 1963 at NASA Conference on Stellar Evolution, New York (in press).
Goldberg, L., Müller, E. A., and Aller, L. H. 1960, *Ap. J. Suppl.*, **5**, 1.
Helliwell, T. M. 1961, *Ap. J.*, **133**, 566.
Herr, W., Hoffmeister, W., Hirt, B., Geiss, J., and Houtermans, F. G. 1961, *Zs. Naturforsch.*, **16a**, 1053.
Hoyle, F., and Fowler, W. A. 1960, *Ap. J.*, **132**, 565.
———. 1963, *Nature*, **197**, 533.
Iben, I., Jr. 1963, *Ap. J.*, **138**, 1090.
König, L. A., Mattauch, J. H. E., and Wapstra, A. H. 1962, *Nuclear Phys.*, **31**, 18.
Kümmel, H., Mattauch, J. H. E., Thiele, W., and Wapstra, A. H. 1964, *Proceedings of the Second International Conference on Nuclidic Masses* (Vienna: Springer-Verlag).
Macklin, R. L., and Gibbons, J. H. 1964, *Rev. Mod. Phys.* (in press).
Mason, B. 1962, *Meteorites* (New York: John Wiley & Sons).
Mottelson, B. R., and Nilsson, S. G. 1959, *Mat. Fys. Skr. Dan. Vid. Selsk.*, Vol. **1**, No. 8.
Nichiporuk, W., and Brown, H. 1962, *Phys. Rev. Letters*, **9**, 245.
Nilsson, S. G. 1955, *Mat. Fys. Medd. Dan. Vid. Selsk.*, Vol. **29**, No. 16.
Reed, G. W., Kigoshi, K., and Turkevich, A. 1960, *Geochim. et Cosmochim. Acta*, **20**, 122.
Ringwood, A. E. 1961, *Geochim. et Cosmochim. Acta*, **24**, 159.
Schmitt, R. A., Bingham, E., and Chodos, A. A. 1964, *Geochim. et Cosmochim. Acta* (in press).
Seeger, P. A. 1961, *Nuclear Phys.*, **25**, 1.
Strominger, D., Hollander, J. M., and Seaborg, G. T. 1958, *Rev. Mod. Phys.*, **30**, 585.
Suess, H. E., and Urey, H. C. 1956, *Rev. Mod. Phys.*, **28**, 53.
Urey, H. C. 1961, *J. Geophys. Res.*, **66**, 1988.
———. 1964, *Rev. Geophys.*, **2**, 1.
Wahlborn, S. 1962, *Nuclear Phys.*, **37**, 554.
Warner, B. 1964, "Barium Stars," *M.N.* (in press).